Ocean Sci. Discuss., 9, 909–975, 2012
www.ocean-sci-discuss.net/9/909/2012/
doi:10.5194/osd-9-909-2012

Ocean Science Discussions

Numerical tools to estimate the flux of a gas across the air-water interface and assess the heterogeny of its forcing functions

V. M. N. de C. da S. Vieira

CCMar–Centre of Marine Sciences, Universidade do Algarve, Campus de Gambelas, 8005–139 Faro, Portugal

Received: 7 February 2012 – Accepted: 28 February 2012 – Published: 12 March 2012

Correspondence to: V. M. N. de C. da S. Vieira (vvieira@ualg.pt)

Published by Copernicus Publications on behalf of the European Geosciences Union.

Abstract

A numerical tool was developed for the estimation of gas fluxes across the air water interface. The primary objective is to use it to estimate CO_2 fluxes. Nevertheless application to other gases is easily accomplished by changing the values of the parameters related to the physical properties of the gases. A user friendly software was developed allowing to build upon a standard kernel a custom made gas flux model with the preferred parametrizations. These include single or double layer models; several numerical schemes for the effects of wind in the air-side and water-side transfer velocities; the effect of turbulence from current drag with the bottom; and the effects on solubility of water temperature, salinity, air temperature and pressure. It was also developed an analysis which decomposes the difference between the fluxes in a reference situation and in alternative situations into its several forcing functions. This analysis relies on the Taylor expansion of the gas flux model, requiring the numerical estimation of partial derivatives by a multivariate version of the collocation polynomial. Both the flux model and the difference decomposition analysis were tested with data taken from surveys done in the lagoonary system of Ria Formosa, south Portugal, in which the CO_2 fluxes were estimated using the IRGA and floating chamber method whereas the CO_2 concentrations were estimated using the IRGA and degasification chamber. Observations and estimations show a remarkable fit.

1 Introduction

The appropriate algorithms for the estimation of gas fluxes across the air-water interface have been the subject of great concern by the scientific community. One of its most notorious applications is in studies about the CO_2 exchange between the atmosphere and the global oceans (Takahashi et al., 2002, 2009) coastal oceans (Frankignoulle, 1988; Frankignoulle and Borges, 2001; Sweeney, 2003; Vandemark et al., 2011), estuaries (Carini et al., 1996; Raymond et al., 2000; Hunt et al., 2011; Oliveira, 2011,

OSD
9, 909–975, 2012

2012), rivers (Cole and Caraco, 2001), lagoons (Sidinei et al., 2001) and lakes (Koné et al., 2009). The marine and aquatic environments may work as either net sinks or net sources of CO_2 for the atmosphere. Nevertheless, this shows a great spatial and temporal variability (Smith and Hollibaugh, 1993; Duarte and Prairie, 2005; Borges, 2005; Borges et al., 2005). The flux of CO_2 across the air-water interface is fundamental to estimate the carbon budget of marine and aquatic ecosystems and classify them as either autotrophic, upon net CO_2 consumption by primary producers, or heterotrophic, upon net CO_2 production by bacterial degradation of organic carbon. Coastal oceans and riverine systems are believed to be globally heterotrophic, remineralizing organic carbon imported from terrestrial ecosystems (Smith and Hollibaugh, 1993; Cole and Caraco, 2001; Duarte and Prairie, 2005; Borges et al., 2005). Although occupying a small fraction of the global ocean the coastal oceans are major sources of CO_2 to the atmosphere, presenting an average CO_2 flux per unit area about 5 times higher than the open ocean (Smith and Hollibaugh, 1993). The flux of a gas across the air-water interface has also been studied for the cases of volatile pollutants, such as organochlorine pesticides, hydrocarbons and heavy metals. These are often imported from industrial and agricultural catchment areas through river basins to the coastal waters of highly populated coastal areas where they may be released to the atmosphere.

There are many physical, chemical and even biological aspects mediating the fluxes of gases across the air-water interface. There is also an extensive literature covering the majority of these aspects. However, very few attempts were made to try and integrate several of these factors, particularly when it involves combining distinct fields of knowledge as chemistry, physical oceanography, meteorology and numerical modelling. Therefore, the first objective of the current work was to develop a numerical tool that provides an accurate estimate of the flux of a gas across the air-water interface, with focus kept on CO_2. This numerical tool was based on that of Johnson (2010) but underwent several upgrades: (i) it is possible to choose between single or double layer models; (ii) new numerical schemes for the effect of wind in the water-phase transfer velocity by Mackay and Yeun (1983), Carini et al. (1996), Raymond and Cole (2001),

OSD
9, 909–975, 2012

Zhao et al. (2003) and Borges et al. (2004b) where introduced; (iii) the effect of sea surface agitation in the water-phase transfer velocity was added; (v) the effect of atmospheric stability in both the air-side and water-side transfer velocities was added; and (iv) the effect in the water-phase transfer velocity of turbulence due to current drag with the bottom following O'Connor and Dobbins (1958) was added. This latter may play a fundamental role in regulating the gas transfer velocity in macro and mesotidal estuarine and lagoonary systems.

The second objective of this work was to develop a numerical method that allows decomposing a difference in the gas fluxes between two distinct situations into the effects of their differences in the environmental variables. This enables the identification of the variables responsible by differences in fluxes between two situations. A good example of the useful application of this new tool is in evaluating the impact of estuarine and lagoonary systems in the CO_2 flux between the atmosphere and coastal waters. This is illustrated with a reference site located offshore and several alternative sites located inside Ria Formosas lagoonary system. The CO_2 fluxes and environmental conditions where determined for all locations and the differences in the CO_2 fluxes and environmental conditions where estimated between the reference site and each of the alternative sites. Another situation where this tool may prove helpful is in the assessment of time dynamics. As an example, if the purpose is to assess the seasonal dynamics, the reference situation should be the climatological average whereas the alternative situations should be the monthly or the seasonally averages. But, if the purpose is to assess the impact of an extreme event as a flood or a drought, the reference situation should be the common environmental conditions whereas the alternative situations should be the specific episode in study.

During the course of this work focus was kept in the CO_2 fluxes. Nonetheless, the numerical tools presented are equally valid for studies of other gases flowing across the air-water interface, substituting the adequate parameters in the model. The current work is intended to set the grounds for further research. This shall consist on including more environmental processes, improve the algorithms of the currently included ones,

OSD
9, 909–975, 2012

submit the tools to a wide range of environmental conditions and to conjugate them with numerical modelling labs such as MOHID, ECO lab, URI's, WRL's or FIO's.

2 State of the art

The flux (mol m^{-2} s^{-1}) of a gas across the air-water interface is usually estimated as in Eq. (1) (or similar formulas), where k (m s^{-1}) is the transfer velocity which often has incorporated the chemical enhancement factor α (scalar), C_a and C_w (mol m^{-3}) are the CO_2 concentrations in the air and water, respectively, and k_H (scalar) is the Henry's constant in its C_a/C_w form. Here, a positive F represents a flux from the air to the water.

$$F = k\left(\frac{C_a}{k_H} - C_w\right) \quad (1)$$

Similar equations have been extensively proposed in the literature (Mackay and Yeun, 1983; Wanninkhof, 1992; Cole and Caraco, 2001; Upstill-Goddard, 2006; Zappa et al., 2007). The gas flux is frequently estimated by the alternative formulation $F = k\alpha\Delta pCO_2$ (Frankignoulle, 1988; Wanninkhof, 1992; Zhao et al., 2003; Borges et al., 2004a,b; Koné et al., 2009; Turk et al., 2010; Hunt et al., 2011) where the CO_2 concentration in the air is given in its partial pressure and the CO_2 concentration in the water is given in its expected air partial pressure would it be at equilibrium with the water and α is Bunsen's gas solubility coefficient, equivalent to Henry's constant (k_H) in its C_w/P_a form. Zhao et al. (2003) calls it s thus preventing confusion with the chemical enhancement factor α. The solubility is required to convert the difference in units of atm to mol m^{-3}. In the works by Raymond et al. (2000), Cole and Caraco (2001) and Vandemark et al. (2011) the ΔpCO_2 is replaced by $\Delta[CO_2]$ the difference between the observed CO_2 concentration in the water and the expected at equilibrium.

The k_H is Henry's constant in its C_a/C_w form, which is a measure of volatility. Historically, it is most famous in its C_w/C_a form or in its C_w/P_a form, becoming a measure of solubility. Sander (1999) and Johnson (2010) proposed algorithms to estimate the

OSD
9, 909–975, 2012

Henry's constant and convert it into its several forms. In order to estimate the effects of water temperature, salinity, air temperature and pressure on solubility/volatility these formulations consider the physical and molecular properties of the air, gas, water and its solvents.

The k term represents the transfer velocity (also known as *piston velocity*) of the gas molecules across the air-water interface. In still air and still water conditions this movement of molecules across the thin layer is due to diffusive transport and thus constrained by the environmental variables that regulate diffusivity. However, when at least one of the phases is not still, turbulence at the interface becomes the main factor regulating the gas transport. The simpler models for the estimation of the transfer velocity consider a single thin layer (Carini et al., 1996; Raymond and Cole, 2001; Borges et al., 2004b; Zappa et al., 2007) across which the transfer velocity equals the water-phase transfer velocity ($k = k_w$). Full explanation of all the algorithms for the k_w estimates would be to extensive and beyond the scope of the current work. In this work, focus is kept in the fundamental physical aspects and the methods to simulate them. A provisional turbulence driven water transfer velocity ($k_w^{\#}$) is estimated as a function of the wind speed (u_{10}) measured 10 meters above water (Liss and Merlivat, 1986; Wanninkhof, 1992; Carini et al., 1996; Nightingale et al., 2000; McGillis et al., 2001; Raymond and Cole, 2001; Borges et al., 2004a,b; Sweeney et al., 2007) or of the air-side friction velocity (u_*) at the air-water interface (Mackay and Yeun, 1983; Zhao et al., 2003) Most often, these are first to second degree polynomials. A constant with the value of 10^{-3} is sometimes added to the $k_w^{\#}$ representing the transfer velocity in still conditions, i.e. the transfer velocity due to diffusivity when wind speed is zero. There are more physical phenomena that affect the water-side transfer velocity and for which have been proposed algorithms to simulate them. Such are the cases of the formation of bubbles with high wind speeds and breaking waves (Memery and Merlivat, 1985; Woolf, 1997, 2005; Zhao et al., 2003; Duan and Marti, 2007), wave field (Taylor and Yelland, 2001; Oost et al., 2002; Fairall et al., 2003; Zhao and Xie, 2010), rain (Ho et al., 2004; Zappa et al., 2009; Turk et al., 2010), surfactants (Frew et al., 2004)

OSD
9, 909–975, 2012

and the variability of the wind velocity over longer time intervals (Wanninkhof, 1992). The parametrization by Fairall et al. (2000) attempts to congregate the fundamental environmental factors over the open ocean.

The provisional water transfer velocity ($k_w^{\#}$) is estimated for fresh water at 20 °C and rectified to the final water transfer velocity (k_w) at actual temperature and salinity multiplying it by the chemical enhancement factor (α). This factor is usually taken as $(Sc_w/600)^{-0.5}$, where Sc_w is the Schmidt number of water estimated for the actual temperature and salinity, 600 is usually accepted as the Schmidt number for fresh water at 20 °C and distinct exponents have been proposed, particularly when related to sea surface agitation or the presence of surfactants. The Schmidt number at actual water temperature and salinity may be given by algorithms of a statistic nature (Carini et al., 1996; Raymond and Cole, 2001; Borges et al., 2004b). These are polynomials that best fitted observations. Alternatively, Johnson (2010) proposed a mechanistic numerical scheme that accounts for the effects of temperature and salinity considering several physical properties, namely the mass fraction of pure water and of the solutes, the water density, the dynamic viscosities of pure water and of the solutes, the kinematic viscosity of water, the mass diffusivity in the water, the molar volume of the gas and of air, and the relative molecular masses of water, of air and of the diffusing gas. The mass diffusivity in the water may be estimated by the algorithms proposed by Hayduk and Laudie (1974), Hayduk and Minhas (1982) and Wilke and Chang (1955). Borges et al. (2004b) proposed adding to the wind driven turbulence the turbulence due to the water current and its drag with the bottom as this may be an important source of turbulence in coastal waters. Its algorithm is given by O'Connor and Dobbins (1958). With these developments the transfer velocity equation used in this work had the general form of Eq. (2). Woolf (2005) further proposed splitting the k_w^{wind} term into a term for sea surface agitation plus a term for whitecap (i.e. bubble formation from breaking waves).

OSD
9, 909–975, 2012

$$k_w = (k_w^{wind} + k_w^{current}) \cdot \left(\frac{600}{Sc_w}\right)^{0.5} \quad (2)$$

Equation (2) is one of the most used formulations for the water-side transfer velocity. It was the adopted in this work and thus was presented with detail. There are nevertheless other two widely used formulations. The Bulk model was implemented in the COARE algorithm (Fairall et al., 1996; Grachev and Fairall, 1997; Fairall et al., 2003) to estimate the fluxes of heat, humidity and gases across the air-water interface, forced by wind, atmospheric stability and sea-surface agitation, and associated to the eddy-covariance field methodology. Surface renewal theory and micro-scale wave breaking congregate a vast body of literature, developed by B. Jähne, E. J. Bock, and associates at the University of Heidelberg and C. J. Zappa, N. M. Frew, W. R. McGillis and associates at the Woods Hole Oceanographic Institution, devoted to the estimation of the transfer velocities of gases, heat and humidity sustained on a common numerical scheme. The work by Frew et al. (2004) relying on such scheme bonds the effects of the main related environmental factors.

A slightly more complex model, the thin film model (Liss and Slater, 1974; Johnson, 2010), also called the two-resistance model (Mackay and Yeun, 1983), considers along the air-water interface both the water-phase and the air-phase thin layers. The final transfer velocity is the weighted harmonic mean of the air-side and water-side transfer velocities, k_a and k_w respectively. Depending on whether the flux is being estimated from the air-side or the water-side point of view, the transfer velocity scheme weights the opposite phase transfer velocity by the Henry's constant. The flux (F) in Eq. (1) is estimated from the water point of view and thus the transfer velocity (k) is estimated as in Eq. (3).

$$k = \left(\frac{1}{k_w} + \frac{1}{k_H \cdot k_a}\right)^{-1} \quad (3)$$

To compute the flux from the air point of view Eq. (4), the transfer velocity must also be estimated from the air point of view Eq. (5). Despite the different transfer velocities the

OSD
9, 909–975, 2012

fluxes yielded by Eqs. (1) and (4) are equal.

$$F = k(C_a - k_H \cdot C_w) \quad (4)$$

$$k = \left(\frac{k_H}{k_w} + \frac{1}{k_a}\right)^{-1} \quad (5)$$

In this *thin film* model the water-phase transfer velocity (k_w) is estimated likewise the transfer velocity in the single thin layer model Eq. (2) whereas the air-phase transfer velocity (k_a) needs a different formulation. The k_a is mainly driven by the wind velocity. Therefore, Duce et al. (1991), Liss (1973) and Shahin et al. (2002) estimate k_a directly from u_{10} whereas Mackay and Yeun (1983), Zhao et al. (2003) and Johnson (2010) estimate it from the friction velocity (u_*). The simplest way to get to u_* from u_{10} is through the drag coefficient: $CD = (u_*/u_{10})^2$. The simplest formulation is by Duce et al. (1991) proposing a fixed value drag coefficient, which has been proved to be unrealistic. A variable drag coefficient dependent on u_{10} was estimated from field surveys (Smith, 1980), wind tunnel experiments (Mackay and Yeun, 1983) and deep water wind seas (Taylor and Yelland, 2001). Sethuraman and Raynor (1975) proposed drag coefficients dependent on the surface roughness and estimated by the Reynolds number, or dependent on the atmospheric stability and estimated by the Richardson number. Air temperature and pressure may also affect the air transfer velocity in a mild manner. Due to that, Mackay and Yeun (1983), Shahin et al. (2002) and Johnson (2010) propose air transfer velocity equations that include temperature and/or pressure dependent terms of the air diffusivity (D_a) and/or the Schmidt number of air (Sc_a).

3 Methods

3.1 The gas flux model

The current work provided a numerical scheme for the estimation of the flux of a gas through the air-water interface, a Matlab® based free open source software package to

OSD
9, 909–975, 2012

implement it and a tutorial for the software; available as online supplementary material (InterfaceGasFlux.zip). The pre-defined gas model constants were those of CO_2. To implement the model with a different gas these constants must be replaced by the appropriate values for the respective gas. The model estimated the gas flux both from the water and the air point of view Eqs. (1) and (4). Therefore, when the double layer model was used the overall transfer velocity was the harmonic mean of the water-side and air-side transfer velocities estimated from the water and the air point of view Eqs. (3) and (5). The flux of a gas across the air-water interface had basically two components (Frankignoulle, 1988):

1. The difference between the gas concentrations in the water and in the air gave the direction of the flux and its strength. It is analogous to the electric potential difference across a membrane or the potential energy of water in an elevated reservoir. Equilibrium was not reached when concentrations were equal but rather when these were at a proportion given by Henry's constants. These were measures of solubility/volatility of the gas in the water and were dependent on temperature, salinity and air pressure. The formulations used for the estimation of Henry's constants were the ones given by Sander (1999) and Johnson (2010), available in the software executable file "kHExe.asv".

2. The resistance of the medium to the vertical movement of matter restricted the gas transfer velocity. This is analogous to the resistivity (or conductivity) of materials to electric currents or of streams to water flow. The model implementation allowed for many options regarding the estimation of the gas transfer velocity. The first one was about choosing between single or double layer models. Then, it was chosen the algorithm for the effect of wind on the water-phase transfer velocity (k_w). The available algorithms were those of Liss and Merlivat (1986), Mackay and Yeun (1983), Wanninkhof (1992), Carini et al. (1996), Nightingale et al. (2000), McGillis et al. (2001), Raymond and Cole (2001), Zhao et al. (2003), Borges et al. (2004b), and Sweeney et al. (2007). The effect on the water-phase transfer velocity of

OSD
9, 909–975, 2012

turbulence from current drag with the bottom following O'Connor and Dobbins (1958) was added. The chemical enhancement of the water-phase transfer velocity (α) was chosen between the algorithms provided by Carini et al. (1996), Raymond and Cole (2001), Borges et al. (2004a) and Johnson (2010). When the latter was chosen it required also choosing the algorithm for the effects of temperature and salinity on water diffusivity. It could be chosen between those provided by Hayduk and Laudie (1974), Hayduk and Minhas (1982) and Wilke and Chang (1955). When the double layer model was chosen it required also choosing the algorithm for the effect of wind on the air-phase transfer velocity (k_a). It could be chosen between those provided by Liss (1973), Mackay and Yeun (1983), Duce et al. (1991), Shahin et al. (2002), Johnson (2010) and Johnson's adaptation of COARE algorithm (Johnson, 2010). Several of the k_w and k_a algorithms relied on the friction velocity, which could be estimated from u_{10} using the CD. The simplest way was to use the fixed drag coefficient proposed by Duce et al. (1991). This was unrealistic and its expected bias was accessed comparing with variable drag coefficient formulations dependent on u_{10} as proposed by Smith (1980), Mackay and Yeun (1983) and Taylor and Yelland (2001). But even these are of limited application and thus the model was upgraded to include the effects of sea-surface roughness and atmospheric stability on the turbulence driven transfer velocities. These are detailed in the remaining paragraphs of this section. The formulations for the estimation of k_w are available in the software executable file "kwExe.asv" whereas the formulations for the estimation of k_a are in "kaExe.asv".

Surface roughness is dependent on the distance the wind has been acting upon the water surface (i.e. the fetch) generating a shear stress. Equivalent winds acting over longer fetches are expected to generate more turbulence and shear stress, and therefore also bigger roughness lengths. The formulation proposed here followed the same rationale as the AERMOD, developed by the Environmental Protection Agency (EPA). The basic principle was to adapt the log wind profile equation solving for friction velocity as a function of wind speed and roughness length. Then, apply this estimate to the

OSD
9, 909–975, 2012

available friction velocity based formulations of air-side and water-side transfer velocities, k_a and k_w respectively. Still, atmospheric stability may also play an important role in the relation of wind speed with friction velocity. Atmospheric stability is a micrometeorological concept related to the buoyancy (advection of warmer air) production of turbulent kinetic energy (see Monin-Obukhov similarity theory). Thus, a more accurate formulation is the log-linear wind profile Eq. (6) named so because it incorporates a logarithmic term for roughness length and a linear term for atmosphere stability:

$$u_z - u_s = \left(\frac{u_*}{k}\right) \cdot \left(ln\left(\frac{z}{z_0}\right) + \Psi(z, z_o, L)\right) \quad (6)$$

Here, u_z ($m\,s^{-1}$) is the wind velocity at height z (m), u_s ($m\,s^{-1}$) is the collinear component of the water current velocity at the sea surface, k is the von Kármán constant (usually 0.4) and z_0 (m) is the roughness length. To avoid confusion it must be noted that z is height in meteorology (presently 10 m) whereas is depth in oceanography; that the current velocity (presently u_s) is referred as w in hydrodynamics whereas w is the vertical wind component in meteorology; and that von Kármán constant (k) should not be confounded with the transfer velocity (k). The atmospheric stability function (Ψ) is given by Eq. (7) according to Sethuraman and Brown (1976) and Woodward (1998), where α is a constant (not to be mistaken for the chemical enhancement factor nor Bunsen's solubility coefficient) usually between 4.5 and 7 for atmospheric stable conditions (Sethuraman and Brown, 1976), L (m) is the Monin-Obukhov length given by Eq. (8), u_* is the friction velocity ($m\,s^{-1}$), ρ is the air density ($g\,m^{-3}$), Θ is the potential temperature of air (K), c_p is the specific heat of air ($J\,g^{-1}\,K^{-1}$), H is the vertical heat flux ($J\,m^{-2}\,s^{-1}$) assumed positive upwards and g is the gravitational acceleration ($m\,s^{-2}$).

$$\Psi(z, z_o, L) = \alpha \frac{z - z_0}{L} \quad (7)$$

$$L = -u_*^3 c_p \rho \Theta (k \cdot g \cdot H)^{-1} \quad (8)$$

OSD
9, 909–975, 2012

The wind log-linear profile was originally developed for air masses over land. Under neutral stability land and air are at the same temperature ($H = 0$, $L = \pm\infty$, $\Psi = 0$) and the wind follows a logarithmic decay as it approaches the soil. When the land is warmer than the air it heats the air immediately above, which flows up generating turbulence and thus increasing the momentum transfer along the atmosphere surface boundary layer. This is an atmospheric unstable condition where the wind log profile is smoothed linearly ($H > 0$, $L < 0$, $\Psi < 0$). Relative to the neutral stability, equivalent winds generate more friction velocity, or equivalent friction velocities require less wind. When the land is colder than the air it cools the air immediately above, stratifying the atmosphere surface boundary layer and thus decreasing the momentum transfer within it. This is an atmospheric stable condition where the wind log profile is enhanced linearly ($H < 0$, $L > 0$, $\Psi > 0$). Relative to the neutral stability, equivalent winds generate less friction velocity, or equivalent friction velocities require more wind. Over land the atmosphere is generally unstable during the day and stable during the night. The wind log-linear profile also takes place over the ocean (Grachev and Fairall, 1997; Mears et al., 2001; Fairall et al., 2003; Lange et al., 2004; Chelton and Freilich, 2005; Hoffman and Leidner, 2005; Capps and Zender, 2009). However, it does not necessarily follow the same daily and/or seasonal variation as over land as the high specific heat of water makes it very resistant to abrupt temperature changes. As an example at Ria Formosa's geographical area the air is warmer than the water during the day for most of the year, but this is reversed during the coldest part of winter. Presently, the log-linear wind profile Eq. (6) was solved for the friction velocity Eq. (9). However, its application presented two major problems. One was the lack of the equipment required for the field estimates of the variables related to the Monin-Obukhov length L. The other was that, because the friction velocity and the Monin-Obukhov length L are dependent on each other, these did not have an exact analytical solution but required being estimated numerically. This should be done iterating Eqs. (7) to (9) for convergence of u_* (see Grachev and Fairall (1997) and Fairall et al., 2003). However, given the present constrains, it was chosen to classify the atmospheric stability accordingly to Pasquill-Gifford's classes and to

OSD
9, 909–975, 2012

correlate these with the expected Monin-Obukhov length L (Woodward, 1998) and α_{AS} (Sethuraman and Brown, 1976)

$$u_* = \frac{(u_z - u_s)k}{ln(z) - ln(z_0) + \Psi(z, z_0, L)} \quad (9)$$

The field estimates of roughness length were done according to Taylor and Yelland (2001) formulation, $z_0/H_s = A(H_s/\Omega L_p)^B$, where H_s (m) is the significant wave height, L_p (m) is the wave length of waves at the peak wave spectrum, Ω is a scaling constant presently introduced, $A = 1200$ and $B = 4.5$. This parameterization predicts the drag coefficient (and thus also the friction velocity and roughness length) increases with increasing fetch and wind duration. Other parameterizations by Donelan (1982, 1990), Smith et al. (1992), Oost et al. (2002) and Fairall et al. (2003) estimate the wave age based on peak wave speed and friction velocity. These were not tested as their requirement for a friction velocity input would return a circular function. The H_s and L_p data were collected by Instituto Hidrográfico's buoy located 6.1 km off shore from Ria Formosa and over 93 m depth.

3.2 Field estimates and units conversions

The gas concentrations are commonly estimated from the field in either mol m^{-3} or ppm units. In the current work was used data with the IRGA and floating chamber sampling procedure, yielding the gas concentrations in ppm. For the current software the gas concentrations could be provided in either form but had to be converted into mol m^{-3} prior to Eqs. (1) and (4). There were two distinct types of conversions: (i) the [gas] in the air converted between ppm and mol m^{-3} using the ideal gas law, and (ii) the [gas] in the water converted between mol m^{-3} and its equivalent air ppm at equilibrium, using Henry's constants. The details on these conversions are provided on Supplement A, together with the protocol for the estimation of the flux from the floating chamber data. Preliminary tests with the model yielded a flux even when the CO_2 concentrations (both given in ppm) in the water and in the air were in equilibrium. It enlightened the need for

OSD
9, 909–975, 2012

careful, accurate conversion between the distinct forms of the Henry's constants. The k_{Hpc} is the Henry's constant for water at 25°C and 0 ppt salinity given in its P_a/C_w form. It has a value of 29.4118. The k_H is the Henry's constant for a given temperature and salinity in its C_a/C_w form. Johnson (2010) presents an algorithm to estimate k_H from k_{Hpc}. This algorithm is represented in the first line of the braced expression in Eq. (10). The $f(T)$ and $f(S)$ represent the functions that resolve for the given temperature and salinity respectively, $T_{K,w}$ is water temperature in Kelvin and α_H is a constant with the value of 12.2. This constant is given by Sander (1999) in an algorithm to estimate k_{Hcp} from k_H (in the second line of the braced expression in equation 10) were $T_{K,a}$ is air temperature in Kelvin. The k_{Hcp} is needed to convert the equilibrium CO_2 concentration in the water from ppm to mol m^{-3} at the given environmental conditions (Eq. A5). However, it is fundamental that the k_{Hcp} estimation for those environmental conditions follow the same algorithm previously used for the k_H estimation for the same environmental conditions Eq. (10). Furthermore, it is also essential to note that the temperature in Sander's Sander (1999) expression is relative to air. This is not explicit in the original article and one may easily be misled assuming it is water temperature because this is the main control of solubility. However, its effect was already accounted for in the k_H estimation from k_{Hpc}. This is demonstrated by developing equation (1) to $C_a/(C_w \cdot k_H) = 1$. If both CO_2 concentrations are given in ppm and their conversions are introduced into this equation, knowing that $P_{(atm)} = 101325.01 Pa$, Eq. (11) is obtained; but only if the temperature in Sander (1999) expression is air temperature. Otherwise, the equation only applies when air and water temperatures are equal. Equation (11) was also used to accurately determine α_H as 12.1866.

$$\begin{cases} k_H = \frac{\alpha_H \cdot k_{Hpc} \cdot f(S)}{T_{K,w} \cdot f(T)} \\ k_{Hcp} = \frac{\alpha_H}{T_{K,a} \cdot k_H} \end{cases} \Rightarrow k_{Hcp} = \frac{T_{K,w} \cdot f(T)}{T_{K,a} \cdot k_{Hpc} \cdot f(S)} \tag{10}$$

$$\frac{C_a}{C_w k_H} = 1 \Rightarrow \frac{101325.01}{10^3 \cdot R \cdot \alpha_H} = 1 \tag{11}$$

OSD
9, 909–975, 2012

3.3 Decomposition of the Difference in the gas Fluxes

For some studies it may be useful to compare a particular case of a gas flux with that of a reference situation, identifying and ranking the causes for the difference. This was illustrated with an example where the objective was to understand how lagoonary systems like Ria Formosa may affect the CO_2 flux in coastal waters. Therefore, the reference situation was the environmental conditions of the oceanic coastal waters and its CO_2 flux, whereas the particular case was the environmental conditions inside Ria Formosa and its CO_2 flux. The environmental conditions of the reference situation were recorded in a column vector x_a and its CO_2 flux was estimated by the numerical model above as f_a. The environmental conditions of the particular case were recorded in a column vector x_b and its CO_2 flux was estimated by the numerical model as f_b. The difference between the environmental conditions of the particular case and of the reference situation (Δx) was given in the column vector $\boldsymbol{h}$ Eq. (12). The column vectors were arranged as $x_1 = C_{air}$, $x_2 = T_{air}$, $x_3 = P$, $x_4 = u_{10}$, $x_5 = z_0$, $x_6 = L_{MO}$, $x_7 = \alpha_{AS}$, $x_8 = C_w$, $x_9 = T_w$, $x_{10} = S$, $x_{11} = w$ and $x_{12} = z_w$. It is important to recognize when subscript *a* stands for air or for the reference situation.

$$h = \begin{bmatrix} h_1 \\ \dots \\ h_i \end{bmatrix} = \begin{bmatrix} x_1 \\ \dots \\ x_i \end{bmatrix}_b - \begin{bmatrix} x_1 \\ \dots \\ x_i \end{bmatrix}_a \tag{12}$$

The difference in the CO_2 flux was given by $f_b - f_a$. It was decomposed into its multiple parcels, each attributable to the difference in a particular environmental variable or interactions between variables. This decomposition was possible developing the Taylor expansion of the gas flux model as in Eq. (13).

$$f_b - f_a = \sum_{n=0}^{\Theta} \frac{1}{n!} \left[\left(h_1 \frac{\partial}{\partial x_1} + h_2 \frac{\partial}{\partial x_2} + \dots + h_i \frac{\partial}{\partial x_i} \right)^n \cdot f_k \right] - f_a \tag{13}$$

The partial derivatives were estimated at point k located within the interval between x_a and x_b. The integer Θ stated the highest order terms used. Usually Θ is high enough

OSD
9, 909–975, 2012

for the remainder to be close to zero. However, as there were many independent variables the number of higher order terms got too big and its estimation turned computationally too heavy. Therefore, the software was developed to automatically adjust this decomposition for a specified number of independent variables, each with its own Θ_i order terms Eq. (14). It started by locating each term of the Taylor expansion in a specified cell entry of a data array (named *TaylorArray*) with *i* dimensions Eq. (15). In this case it was a hyper-volume with 12 dimensions. Afterwards, all terms were summed. The coordinate of each term in each dimension was given by the respective rank of its partial derivative. Computationally, as Matlab® does not accept index zero for arrays, the $\partial^0 x_i$ was placed in the 1st cell, the $\partial^1 x_i$ was placed in the 2nd cell and the $\partial^n x_i$ was placed in the $(n+1)^{th}$ cell along the i^{th} dimension, each being only extended until its own Θ_i term. This procedure enabled a variable-wise sorting out of insignificant terms, optimizing computational effort. The multivariate form of the Taylor expansion has each term preceded by a coefficient given by the multinomial in Eq. (16). However, the numerator in Eq. (16) cancels out with the denominator from the middle quotient in Eq. (15), thus simplifying the calculus Eq. (17). The first entry in the hyper-volume ($TaylorArray_{1,1,\ldots,1}$) had the combination of all the partial derivatives of 0 order, that is: f_a. Therefore, subtracting f_a was done by simply setting this first entry to 0.

$$f_b - f_a = \sum_{n_1=1}^{\Theta_1+1} \sum_{n_2=1}^{\Theta_2+1} \cdots \sum_{n_{12}=1}^{\Theta_{12}+1} \left(TaylorArray_{n_1,n_2,\ldots,n_{12}} \right) - f_a \tag{14}$$

$$TaylorArray_{n_1,n_2,\ldots,n_{12}} = \binom{\sum n_i}{n_1, n_2, \ldots, n_{12}} \frac{\prod h_i^{n_i}}{(\sum n_i)!} \frac{\partial^{\sum n_i} f_{k_1,k_2,\ldots,k_{12}}}{\partial^{n_1} x_1 \partial^{n_2} x_2 \ldots \partial^{n_{12}} x_{12}} \tag{15}$$

$$\binom{\sum n_i}{n_1, n_2, \ldots, n_{12}} = \frac{(\sum n_i)!}{\prod (n_i!)} \tag{16}$$

OSD
9, 909–975, 2012

$$TaylorArray_{n_1,n_2,\ldots,n_{12}} = \prod_{i=1}^{12}\left(\frac{h_i^{n_i}}{n_i!}\right)\frac{\partial^{\sum n_i} f_{k_1,k_2,\ldots,k_{12}}}{\partial^{n_1}x_1\partial^{n_2}x_2\ldots\partial^{n_{12}}x_{12}} \quad (17)$$

The partial derivatives were estimated numerically. While the detailed explanation on the procedure is available in Supplement B, here only a brief overview is presented. The gas flux function was approximated by a collocation polynomial in its turn estimated by a multivariate adaptation of Newton's finite difference formula. The collocation polynomial was partially derived to each of the dimensions. The output was a numerical estimate of the partial derivatives of the collocation polynomial that fitted with accuracy the partial derivatives of the gas flux function for any particular point in the hyper-volume of independent variables.

There were two computationally alternative ways to create the Taylor expansion hyper-volume. One was to go element-wise filling in each entry with the result from Eq. (17). The other was to partition the Taylor expansion hyper-volume into two complementary hyper-volumes: one with the partial derivatives and another with the h_i products and denominators of the multinomial coefficients; and afterwards doing the element-wise product between these two arrays. Each hyper-volume was created starting with a single dimension and expanding dimension-wise until the final twelve dimensional array. In this process each new dimension was added by multiplying the former array by each entry of the new dimension (i.e like the Kronecker product).

Thus far there were too many terms to look at. Ideally it was intended to partition the whole gas flux difference between the independent variables and not between combinations of these variables. In order to achieve this, each multivariate term of the Taylor expansion was itself evenly partitioned among the independent variables that contributed to it. The remainder was estimated subtracting the sum of the estimated terms to the actual gas flux difference given by $f_b - f_a$. It allowed tracking the accuracy of the results, which was one of the criteria used for model optimization. The other was the computational time required to perform the calculus. The model optimization was tested for each dimension at a time and included three features:

OSD
9, 909–975, 2012

1. The order of the partial derivative (Θ_i) worth evaluating. This is illustrated with the simpler situation: if the effect of a variable (x_i) in the gas flux was simulated by a second degree polynomial, it was not worth the inclusion on the i^{th} dimension of the Taylor expansion of the terms with orders (Θ_i) higher than 2 as these did not increased the accuracy of the estimates whereas they did increased significantly the computational effort. Having all the Θ_i set, it was only included in the Taylor expansion the multivariate terms with the crossed partial derivatives with orders up to Θ_1, Θ_2,... and Θ_{12}.

2. The number of steps ahead (n_i) worth taking in Newton's finite difference formula for the collocation polynomial in order to accurately estimate the partial derivative of order Θ_i. In the example above, one step ahead is not enough to accurately estimate a second order derivative but only a first order. Two steps ahead are enough to estimate the second order derivative. More than two steps ahead may (or not) increase the accuracy of the estimates of second order derivatives. Having all the n_i set, for the estimation of the crossed partial derivatives with orders up to Θ_1, Θ_2,... and Θ_{12} were only taken n_1, n_2,... and n_{12} steps ahead.

3. In the process of numerically estimating derivatives, it is crucial the size of the steps taken forward or backward (the δ_i) in Newton's finite difference formula for the collocation polynomial. If these are too large or too small, with increasing order of the terms the δ_i raised to higher powers lead towards infinity or infinitesimal, which turns the error unbearable. A simple, direct answer to this problem was choosing the δ_i to always be in the vicinity of 1. However, it was not the end of the problem as for some variables, their increase in steps of size 1 would get them out of bounds, that is, far out of the interval given by $x_{i,\mathrm{a}}$ and $x_{i,\mathrm{b}}$. Thus, it was also necessary to play with the units upon which the steps were taken so that they would be within bounds but still represented by numbers with one digit: (a) gas concentrations could be converted from $\mathrm{mol\,m^{-3}}$ into $\mathrm{mmol\,m^{-3}}$; (b) air pressure from atm into kilopascal (KPa); (c) wind speed from $\mathrm{m\,s^{-1}}$ into $\mathrm{Km\,h^{-1}}$;

OSD
9, 909–975, 2012

(d) roughness length from m into dm, cm, mm or 10^{-1} mm; (e) L_{MO} from m into dam, (f) α_{AS}, a scalar, into ·10 units, (g) current speed from m s^{-1} into dm s^{-1}, cm s^{-1}, m min^{-1}, hm h^{-1} or km h^{-1}; and (h) depth from m into dm, dam or hm.

The last problem needed to be solved concerned the [gas] when supplied in units of ppm to a model that works with units of mass volume^{-1}, and the existence of a temperature and/or pressure difference between reference and alternative sites. In order to clearly illustrate this issue, consider a reference and alternative sites that were equal in every variable except air pressure. In this case the reference and alternative sites have equal [gas] when expressed in units of ppm. Then, the two sites exhibited a difference in [gas] when expressed in units of mass volume^{-1} simply because equal amounts of gaseous mass occupy different volumes when subject to different pressures. The preliminary DDF did not consider the effect on the gas flux of this [gas] difference induced by the air pressure. Therefore, there was a part of the flux that was not considered. The DDF was upgraded by rectifying the numerical estimates of the partial derivatives: when the [gas] were given in ppm it was not automatically converted to mol m^{-3}. First, the steps further were taken in Newton's finite difference formula with the [gas] still in ppm units as these were equally well suited for that purpose. Only after each step was taken the respective ppm was converted to the mol m^{-3} that was fed to the flux model. This procedure enabled to account for the effects of air temperature and pressure variations on the conversion of the gas concentrations.

4 Results

In order to compare the performance of the flux formulations an environmental reference situation was set where the variables had fixed values. Then, the effect of each environmental variable was tested independently by changing each variable at a time. C_a was fixed at 370 ppm; T_a was tested from 0 to 40 and fixed at 20 °C; P was fixed at 1 atm; u_{10} was tested from 0 to 30 and fixed at 0.001 m s^{-1}; z_0 was tested from 10^{-5} to 10^{-1} and fixed at 10^{-5} m; the Monin-Obukhov length (L_{MO}) was tested from $^{-}0$ to $^{+}0$

OSD
9, 909–975, 2012

and fixed at ∞; C_w was tested from 200 to 900 and fixed at 370 ppm; T_w was tested from 0 to 30 and fixed at 20 °C; S was tested from 0 to 40 and fixed at 0 ppm; w was tested from 0 to 2 and fixed at 0.001 m s^{-1}; z_w was tested from 0.5 to 10 and fixed at 10 m.

4.1 Air-side transfer velocity

Wind was one of the most influential environmental factors affecting the air-side transfer velocity. Several algorithms simulating this relation are presented in Fig. 1. All the equations about the wind effect including a term for the drag coefficient (Johnson, 2010; Mackay and Yeun, 1983) were very coherent among each other. As expected, the Duce et al. (1991) constant drag coefficient underestimated the air transfer velocity at high wind speeds relative to the drag coefficient parameterizations by Smith (1980) and Mackay and Yeun (1983). Furthermore, this parameterization passed through the origin, meaning no CO_2 flux at still air. Other formulations presented the same problem, as was the case of the COARE formulation by Jeffrey et al. (2010). In the COARE algorithm this was solved with the addition of a gustiness term (Grachev and Fairall, 1997; Fairall et al., 2003). Presently, this was solved with the addition of a constant (10^{-3}) following Mackay and Yeun (1983) and Johnson (2010). After wind, roughness length and atmospheric stability were the next most influent parameters in the air-side transfer velocity (Fig. 2). However, accounting for these required using the k_a formulations dependent on friction velocity, which in its turn was no longer dependent on the drag coefficient formulation but on the wind log-linear profile. The scheme used in Fig. 2, by Mackay and Yeun (1983), was fit to wind tunnel data and thus, in the absence of long fetches (and therefore of rough surfaces) and under neutral atmospheric stability. However, when these effects were added the k_a predictions increased significantly. It became close to the highest predicting k_a formulations and apart from the bulk of the k_a estimates without roughness length and atmospheric stability. Only the algorithm by Shahin et al. (2002) simulated perceptible effects of air temperature and pressure on k_a (Fig. 3), but even this was relatively meaningless compared to the wind effect.

OSD
9, 909–975, 2012

4.2 Water-side transfer velocity

The water diffusivity equations yielded approximate results with water temperature changing from 0 °C to 30 °C (Fig. 4,up). Thus, choosing different diffusivity equations had little effect on both the Schmidt number of water (Sc_w) and the chemical enhancement factor (α) when estimated according to Johnson (2010). Other α algorithms by Borges et al. (2004b), Carini et al. (1996) and Raymond and Cole (2001), which did not account for diffusivity, also yielded approximate results with changing temperature (Fig. 5,up). The Carini et al. (1996) and Raymond and Cole (2001) algorithms share the same equation for the estimate of α and thus their lines were over imposed. All these algorithms yielded α very close to 1 in fresh water at 20 °C as it was supposed to be. The estimates of the effect of salinity in both the water diffusivity (Fig. 4,down) and α (Fig. 5,down) were also very approximate, apart the Carini et al. (1996) and Raymond and Cole (2001) algorithms, which did not account for salinity in the α estimate and thus their lines were horizontal and over imposed.

When comparing the several available algorithms for the relation of wind speed with k_w^{wind}, two groups were set aside (Fig. 6). The first group had the algorithms developed for open ocean estimates and/or strong winds. The relations were exponential and maybe underestimated k_w at low winds due to the lack of data. Inside this group, the McGillis et al. (2001) algorithm was clearly exaggerated relative to the remaining algorithms. The formulation by Mackay and Yeun (1983) was estimated in a wind tunnel with wind speeds between 5 and 22 m s^{-1} and extrapolated for environmental conditions using the wind dependent drag coefficient scheme by Smith (1980). The constant drag coefficient (Duce et al., 1991) and the wind dependent drag coefficient estimated from wind tunnel experiments (Mackay and Yeun, 1983) were discarded. The second group had the algorithms developed from river and estuarine surveys in low wind regimes. The Carini et al. (1996) and Borges et al. (2004b) functions were linear. Thus, though the k_w^{wind} at low winds were probably closer to reality, at high winds were underestimated. The Raymond and Cole (2001) was an exponential function

OSD
9, 909–975, 2012

estimated exclusively from wind speeds below 8 m s^{-1}. Its extrapolation to high winds was a wild guess yielding the fastest transfer velocities.

Roughness length and atmospheric stability had a remarkable influence in the water-side transfer velocity (Fig. 7). However, these required using the k_w^{wind} formulations dependent on friction velocity, which in its turn was no longer dependent on the drag coefficient formulation but on the wind log-linear profile. Rougher sea-surfaces (with higher roughness lengths) created more wind drag and therefore increased friction velocity. Atmospheric instability increased the momentum transfer across the atmospheric boundary layer, thus also increasing the friction velocity: wind speed decayed less from u_{10} till the sea-surface. Atmospheric stability stratified the atmospheric boundary layer decreasing the momentum transfer across it, thus decreasing the friction velocity: wind speed decayed more from u_{10} till the sea-surface. The scheme used in figure 7, by Zhao et al. (2003), when the effects of roughness length and atmospheric stability were added matched the formulations developed for open ocean and from moderate to high wind experiments.

Only one algorithm, by O'Connor and Dobbins (1958), was used to estimate the effect of water current and depth on the water-side transfer velocity ($k_w^{current}$). The transfer velocity increased non-linearly with increasing water current and decreasing depth (Fig. 8). Its magnitude was similar to the magnitude of the water transfer velocity imposed by low to moderate winds.

4.3 The gas flux

The direction of the CO_2 flux across the air-water interface shifted around the equilibrium point with variable CO_2 concentrations in the water (Fig. 9). The steepness of the slopes showed the sensitivities of the flux algorithms to the gas concentrations. These slopes varied greatly with wind speeds, reflecting the fundamental role of wind in the flux of a gas across the air-water interface through its effect in the transfer velocity. The influence of water temperature and salinity on the CO_2 flux was estimated with

OSD
9, 909–975, 2012

the temperature set to 17.38 °C (Fig. 10). This is the water temperature at which the Henry's constant equals 1 for a 0 ppt salinity and 1 atm air pressure. The CO_2 concentrations in mol m^{-3} in the x axis correspond to the CO_2 concentrations of 200 to 900 ppm in water at 17.38 °C and 0 ppt. Water temperature and salinity had a dual effect in the CO_2 flux across the air-water interface. The changes in the y intercept were due to their effects in the solubility of CO_2 (k_H), whereas the steepness of the slopes were given by their effects in the water-side transfer velocities (Fig. 10,up). The same test was done isolating the ΔCO_2 term (Fig. 10,down). Water temperature and salinity only affected the y intercept of the functions due to their effects in the solubility of CO_2. All slopes exhibited the same steepness as the transfer velocity was not included in the function. A fairly similar process occurred with the effects of air temperature and pressure on the CO_2 flux and on the ΔCO_2 (Fig. 11), but only when the CO_2 concentrations in at least one of the phases was given in units of ppm and thus required conversion to mol m^{-3}. In such cases changes in the air temperature and/or pressure changed both the slope and the y intercept of the function.

4.4 Model application

The model was tested by comparing the CO_2 flux estimates with the CO_2 fluxes observed in Ria Formosa's main channels and at the nearby coastal ocean with the IRGA and floating chamber technique (Fig. 12). The model estimates were forced by the data on the environmental variables that were simultaneously collected. Data was not available to allow for estimates of roughness length inside Ria Formosa. Therefore, given the calm weather and smooth sea surface, these were arbitrarily given the value of $z_0 = 10^{-4}$ m (see Mackay and Yeun (1983) and Vickers and Mahrt (2006)). The fit between the predicted CO_2 fluxes and the observed inside Ria Formosa was good irrespective of the sea-state and atmospheric stability formulations. However, for the nearby coastal ocean the inclusion of these factors was crucial for predictions to fit the observations (in Fig. 12 and a few more unpublished data). Using the adapted Taylor and Yelland (2001) formulation with $A = 1200$, $B = 4.5$ and $\Omega = 1$ yielded roughness

OSD
9, 909–975, 2012

lengths around 10^{-7}m to 10^{-6}m and very poor fits (not shown). These improved significantly when an $\Omega = 0.355$, $A = 1.26$ and $B = 1.2$ where used. There was no field data available to allow for an objective estimation of the effects of atmospheric stability on the CO_2 flux during the field surveys. Therefore, the L_{MO} and α_{AS} where arbitrarily chosen following Sethuraman and Brown (1976) and Woodward (1998). With the water temperature about 4 °C higher than the air temperature on the 3 March it was decided to arbitrarily attribute a Pasquill-Gifford slightly unstable condition with $L_{MO} = -14$ and a stability $\alpha_{AS} = 3$. On the other hand, the water temperature was about 4 °C lower than the air temperature on the 14th of April and about 1 °C on the 15 April, and therefore it was decided to arbitrarily attribute Pasquill-Gifford slightly stable conditions with respectively $L_{MO} = 40$ and a stability $\alpha_{AS} = 6$, and $L_{MO} = 70$ and a stability $\alpha_{AS} = 4.5$. These values were chosen a priori. This exercise demonstrated the sea-state and atmospheric stability were important factors affecting the CO_2 flux during the coastal ocean surveys. Changing from the Mackay and Yeun (1983) k_w^{wind} formulation to the Zhao et al. (2003) formulation turned the fit almost into a perfect match suggesting whitecap was fundamental at setting the water-side transfer velocity. The overall transfer velocity was always limited by the water-side transfer velocity as the air-side transfer velocity was one order of magnitude faster (Fig. 13).

The ΔCO_2 in Ria Formosa's water body showed a pattern much similar to the CO_2 flux (Fig. 14) still, with a smoother variation. Here, positive values represent depletion (forcing uptake) whereas negative values represent surplus (forcing escape) of CO_2 in the water relative to what would be expectable if it was in equilibrium with the overlying atmosphere. It was evident the heterogeny of the Ria Formosa water body in terms of CO_2 budget. In March it was behaving autotrophically, with a depletion of CO_2 relative to the atmosphere whereas in April it showed an erratic behaviour, changing from autotrophic to heterotrophic in just a few hours.

OSD
9, 909–975, 2012

4.5 Tuning the decomposition of the difference in the gas fluxes

The DDF analysis must be optimized before its application with the intention to minimize both the error in the estimates and its computational effort. This includes choosing for each of the tested variables (x_i) the order of the partial derivatives (Θ_i), the size (δ_i) and number (n_i) of the steps taken, and the point of estimation of the partial derivatives (k_i) in units of steps from $x_{i,a}$. Knowing the computational effort and the error in the estimates are inversely proportional it was searched for the right balance. The inference of the best options was summarized in Table 1 and figures (15) and (16). The cpu time was estimated for the n_i steps in the tested variable with $n_i = 1$ for all other variables. Not all possible model variables were tested but only the ones currently used for the CO_2 flux estimates. The water temperature was set aside in figure 15 to exhibit a graphical representation of the typical evolution of the error. For this variable, as well as others like air temperature, salinity and wind speed, the optimal choices depended on the algorithms used. This work provides many optional algorithms and it was not feasible to test them all. Only a few were tested and presented in the results. This does not mean these few were the best at estimating the CO_2 flux and should always be preferred. The optimization process also diverged whether the CO_2 concentrations were given in units of ppm or mol m^{-3}. Generally, using the mol m^{-3} units gave more accurate or equally accurate results and with less effort, the exception being with air temperature where it was the other way around.

Fitting the gas flux to the L_{MO}, α_{AS}, z_0, w and z using a multivariate collocation polynomial was only accurate if the n_i steps of size δ_i closely covered the range (Δx_i) between the reference ($x_{i,a}$) and alternative ($x_{i,b}$) situations. It was essayed to feed the z_0, w and z to the DDF tool in several units while adjusting the size and number of steps taken so that δ_i would always be close to 1. There was no globally better solution. In the examples shown in Table 1 the best options were to give w in hm h^{-1} and taking 5 steps of size 3.6, z in dam (10 m) and taking 5 steps of size 1.29, and z_0 in mm and taking 1 step of size 8.9.

OSD
9, 909–975, 2012

It was tested for the optimal point of estimation of the partial derivatives; that is, how far away from $x_{i,a}$ could the partial derivatives be estimated (Fig. 16). This distance is k_i in the collocation polynomial and is given in units of steps taken away from $x_{i,a}$. The k_i need not be an integer number, as it was proved by testing it from 0 to 5 at 0.2 increments. The results are presented for the *easy* variable u_{10} and three harsh variables T_w, w and z. The partial derivatives of the easy variable could be equally well estimated at any k_i within the bounds of $x_{i,a}$ and $x_{i,b}$. On the contrary, the partial derivatives of the harsh variables could only be well estimated at $k_i = 0$.

The optimal point of estimation for the partial derivatives was tested upon and alternative situation: on the available data set it was considered $x_{i,a}$ as the minimum x_i and $x_{i,b}$ as the maximum x_i, over all samples. Then, it was tested whether it was possible to accurately estimate the partial derivatives at point $x_{i,c}$ so that ${}_{\min}x_i \leq x_{i,c} \leq {}_{\max}x_i$, inputting k_i in units of steps of size δ_i taken from ${}_{\min}x_i$ (i.e $k_i = (x_{i,c} - {}_{\min}x_i)/\delta_i$), and as long as δ_i was always customized so that $\delta_i \cdot n_i = {}_{\max}x_i - {}_{\min}x_i$. The $n_{11} = 5$ was important for the accuracy of the estimates of the partial derivatives related to w. The accuracy was generally remarkable (Fig. 17). Nevertheless, for the *harsh* variable of current velocity there were still a few cases for which they were very poor. This error was not due to the method being tested but rather due to the independent estimation of the partial derivatives, used for the comparison: whenever $x_{i,c}$ was to close to ${}_{\min}x_i$ or ${}_{\max}x_i$ it forced δ_i to be much smaller than 1, bringing severe error to these estimates.

4.6 Applying the decomposition of the difference in the gas fluxes

The decomposition of the difference between the CO_2 fluxes in the air-water interface inside Ria Formosa at the 15 April 2011 for the first sample in the time series and in the nearby coastal ocean at the 3 March 2011 (Fig. 18) had only a 0.04 % error relative to the CO_2 fluxes predicted by the model. This is the remainder of the Taylor expansion, i.e. the error specific to the DDF tool. Still, it is known the flux predicted for the 3 March was underestimated by about 2.5 mmol m^{-2} d^{-1}. Therefore, at least for a few variables their actual terms were larger than the ones presented. The CO_2 flux was

OSD
9, 909–975, 2012

positive in the coastal ocean, meaning CO_2 uptake, whereas it was negative inside Ria Formosa, meaning CO_2 escape from the water to the atmosphere. As the coastal ocean was the reference situation (f_a), and Ria Formosa the alternative situation (f_b) the difference ($f_b - f_a$) was negative. The biggest contributor to this difference was the CO_2 concentration in the water (C_w) as the coastal ocean was behaving autotrophically at the 3 March and Ria Formosa was behaving heterotrophically at the 15 April, at least at that section and between 11:00 h and 13:00 h. A smaller CO_2 concentration in the air (C_a) over Ria Formosa also gave a significant contribution to the CO_2 flux difference. The air (T_a) and water (T_w) temperatures, salinity (S) and air pressure (P) had only slight influence on the flux difference. The wind velocity (u_{10}) had a small negative term because it was slightly windier on the 15 April (4.5 m s^{-1}) than on the 3 March (3 m s^{-1}). Nevertheless, the coastal ocean surface was much rougher (z_0) than the water surface at the lagoonary system, generating a much higher k_w^{wind} and thus the large z_0 positive term. Also, the general wind transferred more momentum to the air in contact with the coastal ocean surface given the atmospherically unstable conditions verified at the 3 March 2011 than to the air in contact with the Ria Formosa water surface given the atmospherically stable conditions verified at the 15 April 2011. Thus, the positive terms for L_{MO} and α_{AS}. It was assumed the misfit between the observed and predicted CO_2 fluxes at the coastal ocean was due to the underestimation of z_0, L_{MO} and/or α_{AS}. Therefore, it was expected the actual DDF terms for at least some of these variables to be larger. These positive terms discount from the overall negative sum meaning that if the Ria Formosa at the 15 April had its water surface as rough and the overlying atmosphere as unstable as the coastal ocean had on the 3 March, the CO_2 flux difference would be even higher as there would be more transfer velocity and thus more CO_2 being transferred to the air over Ria Formosa. Nevertheless, inside the lagoonary system the turbulence from below, that is from current drag with the bottom, compensated for the lesser turbulence from above, as it is shown by the negative terms relative to current velocity (w) and depth (z).

OSD
9, 909–975, 2012

5 Discussion

5.1 Model implementation

The application of the present model to estimate the CO_2 flux across the air-water interface showed the overall transfer velocity to be limited by the water-side transfer velocity. This is the expected for sparingly soluble gases such as CO_2 (Upstill-Goddard, 2006; Johnson, 2010). In this case the inclusion or not of the air-side transfer velocity and the choice of its formulation were irrelevant. The fundamental aspect was the water-side transfer velocity and the algorithms chosen to simulate it. On the contrary, for gases that are very soluble or react with water the air-side transfer velocity is expected to be the limiting factor (Upstill-Goddard, 2006). In these cases the inclusion of the air-side transfer velocity should be crucial to accurately simulate the gas fluxes. Sander (1999) provides an extensive list of gases and their solubility in water. The estimation of the overall transfer velocity by the harmonic mean of the air-side and water-side transfer velocities weighted by the gas solubility Eqs. (3 and 5) proved to be an effective way to simulate this dynamics.

Many different algorithms are available on the literature to estimate the water-side transfer velocities. The simpler ones are empirical formulations relating to the effect of a single factor as wind, whitecap or current. Allowing for a variable drag coefficient dependent on wind speed, sea-surface agitation and other physical properties of the atmosphere and ocean (Sethuraman and Raynor, 1975; Smith, 1980; Mackay and Yeun, 1983; Smith et al., 1992; Taylor and Yelland, 2001) increases substantially the model accuracy. It is equally important to consider the advective components of k_a and k_w tend asymptotically to zero as the atmosphere changes to still air and the sea changes to still or deep water, the diffusive transport becoming the dominant feature. Therefore, any model parametrization meant to be applied to coastal studies and inland waters, where low wind is frequent, should account for the diffusive component of k_a and k_w and hence force them to stabilize in accurate values as turbulence decreases. However, most of the available formulations either neglect the diffusive transport or

OSD
9, 909–975, 2012

show great discordance about their related transfer velocities, revealing the lack of care this subject has been devoted.

Wind based algorithms developed from open ocean data are usually second or higher order polynomials that increase the transfer velocity enormously with wind speed. Still, there is great variability within this set of algorithms. The wind based algorithms developed for coastal systems by Carini et al. (1996) and Borges et al. (2004b) are linear functions that underestimate the transfer velocities at high wind speeds due to the lack of such data. Raymond and Cole (2001) fit an exponential function to data from estuaries collected at low winds. Extrapolation to high winds yielded transfer velocities outstandingly higher than any other, even for open ocean. This is probably the best demonstration that the application of many transfer velocity algorithms should be restricted to the specified environmental conditions upon which they were developed.

Slightly more elaborated algorithms integrate the effects of a few factors, allowing for an increase in their applicability and accuracy. However, most of these are still empirical relations constrained to the environmental range upon which they were tested. Considering the broad applicability to the coastal ocean, rivers, estuaries and lagoonary systems it is relevant that only the numerical schemes by Borges et al. (2004b) and Johnson (2010) comprise the effect of salinity changes and only the one by Borges et al. (2004b) import the effects of current drag from previous authors. A few numerical schemes have gone further with more mechanistical approaches to the environmental processes they are representing. This allows for a significant increase in their applicable environmental range and possible interaction with complementary formulations. It is the particular case of Memery and Merlivat (1985), Johnson (2010), the COARE algorithm and the vast body of literature related to the surface renewal theory and micro-scale wave breaking.

The present numerical scheme tries to incorporate all these options and develop a software able to estimates the gas flux across the air-water interface under the broadest range of environmental conditions with a unique model parametrization.The estimates of the water-side transfer velocity showed that in shallow coastal waters the effect of

OSD
9, 909–975, 2012

water current can be as important as the effect of low to moderate winds. In macro and mesotidal estuarine and lagoonary systems higher tidal driven water currents occur on a daily basis, whereas high winds do not. Therefore, the effects of water current and depth are fundamental for the model performance in coastal environments. On the other hand, the attempts to calibrate the model for the coastal ocean samples demonstrated the roughness length and atmospheric stability are key features in the estimation of the gas fluxes across rough water surfaces. Any algorithm that simply considers a drag coefficient dependent on wind speed shall often fail. Therefore, replacing the empirical drag coefficient formulations by a more complex one involving wind, roughness length and atmospheric stability brings the model closer to reality enhancing its accuracy enormously.

The roughness length formulation by Taylor and Yelland (2001) is very practical as it requires only two parameters from the wave field. It is also very intuitive as it states the roughness length scaled to the wave height is proportional to the wave slope, this function being linear or exponential depending on the exponent (B) value. However, the wave fields are not uniform and may be decomposed into a wave spectrum where each of its components potentially gives a relative contribution to the roughness length. The alternative proposed by Taylor and Yelland (2001) is to use the peak component of the wave spectrum. This simplification may imply loss of information and predictive power. However, Moon et al. (2004) have demonstrated for tropical cyclones the Charnock coefficient is mainly determined by wind speed and the peak wave age, thus supporting such simplification. This problem is aggravated by the fact that roughness length is a theoretical concept that can not be tested directly. Usually are used proxies such as the friction velocity, the drag coefficient or the Reynolds number (Sethuraman and Raynor, 1975; Taylor and Yelland, 2001; Fairall et al., 2003; Frew et al., 2004; Moon et al., 2004).

Atmospheric stability is another fundamental aspect in the estimation of a gas flux across water surfaces. The present simulations have demonstrated it to have a huge potential to influence the friction velocity and therefore the transfer velocity.

OSD
9, 909–975, 2012

Sethuraman and Raynor (1975) had already proved it through the drag coefficient. Although the subject of atmospheric stability was originally developed for air over land, Sethuraman and Raynor (1975) have proved the drag coefficient decreases with an increase of the difference between air and water temperatures (that is $T_a - T_w$) corresponding to atmospherically stable conditions. For the 3 March measurements at the coastal ocean the temperature difference was −4 °C, which scaled to the air temperature was −0.33 °C, corresponding to atmospherically unstable conditions. Using Sethuraman and Raynor (1975) linear fits yielded a drag coefficient of 3.91, which is 2.44 times higher than the drag coefficient at equilibrated air and water temperatures. It resulted in friction velocities 1.44 times bigger and predicted CO_2 fluxes 1.52 times bigger when using the Mackay and Yeun (1983) formulation. Nevertheless, the evaluation of atmospheric stability and its application to marine coastal environments should be cautious as Vickers and Mahrt (2006) propose that (i) Monin–Obukov similarity theory does not apply to sea surfaces with sharp temperature gradients and (ii) the sensible heat flux is better correlated with the sea surface temperature in a 1–2 km downstream lag.

Under high winds the effects of whitecap and bubbles become important (Memery and Merlivat, 1985; Zhao et al., 2003; Woolf, 2005) and therefore should be added to the model. Memery and Merlivat (1985) propose a complex algorithm that accounts for many physical properties of water and bubbles. Woolf (2005) states the water-side transfer velocity as the addition of a term for the breaking waves and another for non-breaking waves. Presently it was only implemented the simpler solution by Zhao et al. (2003). It is debatable whether this formulation should or not be overlapped with the roughness length formulation as ultimately both account for the effect of the wave field in k_w^{wind} and therefore may be redundant. In the preliminary test performed in this work their overlap gave the best results, far beyond any other.

In the coastal ocean, as the swell approaches the shore the drag with the shallower bottom compact the waves, decreasing the wave length while keeping the wave height. The wave slope increases and thus also the roughness length (Taylor and Yelland,

OSD
9, 909–975, 2012

2001). Therefore, these authors expect the gas transfer velocity to increase as the coastal ocean approaches the shore. This has two implications for the current work. One is that the data from field surveys or oceanographic numerical laboratories should not neglect the effect of increasing wave slope whit decreasing depth. The other is to clarify that the surface roughness in Ria Formosa is generated exclusively inside the lagoon and independent from the swell outside. Nevertheless, it should be considered the possibility the downwind depth profile inside estuarine and lagoonary systems may have an effect in roughness length and consequently in the gas transfer velocity, as Upstill-Goddard (2006) proposes for generalized shallow waters. Also the presence of surfactants decreases the gas transfer velocity (Memery and Merlivat, 1985; Frew et al., 2004), particularly with lower wind speeds, and surfaces with shorter waves are more affected by surfactants (Frew et al., 2004). Therefore, a likelier presence of surfactants inside estuaries and lagoons than in the nearby coastal oceans should also be considered.

Finally, the current software allows for the gas concentrations to be input in units of ppm although the model requires them to be converted to units of mol m^{-3}. This conversion is dependent on temperature, pressure and salinity, and thus is yet another way to account for the effects of these variables in the flux of a gas across the air-water interface. This is not a model artificialization but rather represents simple objective environmental features. Taking the example of the atmosphere, as an air mass changes its density it keeps its inner relative gas concentrations (given in ppm) but changes its volumetric gas concentrations (given in mol m^{-3}), thus affecting its gas exchanges with any other distinct entity.

5.2 Model alternatives

The quantification of the effects of surface roughness both in the air-side and water-side transfer velocities was done using the Wind log-linear Profile and the variable roughness length (z_0) allowing the estimation of different friction velocities for equivalent wind

OSD
9, 909–975, 2012

speeds. Its accurate estimation requires the effects of atmospheric stability, which requires the quantification of either the Monin-Obukhov length (L) or its related stability parameter (ζ) (Sethuraman and Raynor, 1975; Sethuraman and Brown, 1976; Grachev and Fairall, 1997; Fairall et al., 2003; Lange et al., 2004). Both these variables require data collected by either the eddy covariance or the gradient field methods. However, only the eddy covariance related algorithms allow a model structure that can interact with oceanographic and meteorological numerical labs to estimate atmospheric stability and gas transfer velocities from numerical simulations. The gradient method only allows for model calibration and validation from field data.

Alternatively, it could have been used the Sethuraman and Raynor (1975) formulation describing the drag coefficient dependence of sea surface roughness or the Frew et al. (2004) transfer velocity formulation where it is the exponent upon the Schmidt number to show a dependency on sea surface roughness. Both these formulations present three distinct equations for smooth, moderately rough and fully rough sea surfaces, disabling their application to the DDF tool to compare between pairs of situations which are very distinct in sea surface roughness. There are several methodologies for an indirect estimation of roughness length from the wave field. Presently, was used Taylor and Yelland (2001) formulation relating surface roughness to the wave slope. Frew et al. (2004) and Hwang (2005) present alternative formulations based on the Mean Square Slope. The latter further proposes intermediate scale waves are the dominant contributors to the ocean surface roughness. The wave slope may be estimated using a pressure transducer. However, in the smooth surfaces that often occur in estuarine and lagoonary systems under calm weather are required pressure transducers with resolutions higher than 4 Hz. Alternatively, the wave field may be estimated using a scanning laser slope gauge (Frew et al., 2004).

Friction velocity may be estimated solely from the roughness length following Charnock's model (Charnock, 1955): $z_0 = \alpha_c u_*^2/g$, where α_c is Charnock's coefficient. This alternative implies estimating α_c as a function of u_{10} and the input wave age (Moon et al., 2004). From micro-meteorology theory the friction velocity may also be

OSD
9, 909–975, 2012

estimated from the near surface covariance of horizontal (u′) and vertical (w′) wind components. Then, the gas flux model and DDF analysis must account for friction velocity directly and in replacement of roughness length (z_0) and wind speed (u_{10}). For the model estimation the calculus is simpler as it is a simple function of the horizontal and vertical variability of the wind components. Nevertheless, as for all the alternatives presented that require simpler calculus, these have the cost of information being lost for the DDF analysis. For the example shown in this work it would not be possible to access whether (or how much) of the difference between the CO_2 flux inside the lagoon and in the coastal ocean was either due to the difference in the wind properties or due to the difference in the sea surface roughness.

The total transfer velocity of a gas may also be estimated from the total transfer velocity of heat (Frew et al., 2004). The relation is given by $k_{gas} = k_{heat}(Sc/Pr)^{-n}$, where Sc is the Schmidt number, Pr is the Prandtl number and n is a scalar (usually between 0.5 and 0.7). In its turn $k_{heat} = j_{heat}/(\rho c_p \Delta T)$, where ρ and c_p are seawater density and specific heat, respectively; ΔT is the seawater temperature difference between the "cool skin" and the bulk of the surface boundary layer, which may be estimated from infrared imagery; and j_{heat} is the net heat flux density at the sea surface, which may be estimated from micrometeorological measurements.

Future developments of the numerical scheme should include more algorithms for the effects of current velocity, depth, fetch, breaking waves and surfactants in the water-side transfer velocity, and for the effects of bacterioneuston in the concentration of a gas in the thin surface microlayer. It should also be implemented different solutions for the integration of distinct environmental factors, as are the cases of the COARE algorithm, the surface renewal and micro-scale wave breaking related algorithms or the work by Duan and Marti (2007). It would be interesting to compare gas flux estimates by the floating chamber methodology and the eddy-covariance methods. The required equipment is common to both, allowing for the collection of data about air and water partial pressures of the gas , air temperature and pressure, wind speed, friction velocity and atmospheric stability. The equipement consists of a fast response IRGA (as the

OSD
9, 909–975, 2012

Li-Cor 7500A, EC150 or IRGASON) and 3D sonic anemometer with recording rates ≥5 Hz. This should be useful for equipment optimization and costs reduction.

5.3 Tuning the decomposition of the difference in the gas fluxes

When performing the DDF its optimization is a fundamental part of the process. It is intended to have the most accurate results, still, not wasting time estimating useless steps. If only one step was taken for each variable, estimating only first order partial derivatives, computation would be very fast but the error would be big. On the other hand, if five steps were taken for each variable, estimating the partial derivatives up to the fifth order in each variable, the error would be negligible but the calculus would take forever. The DDF optimization analysis demonstrated the the importance of choosing the order of the derivatives, their point of estimation and the number and size of the steps taken. It further demonstrated that generally it is not worth taking more steps than the optimal order of the partial derivative. The optimal choices varied with the numerical options but also with the units used to give the CO_2 concentrations. This latter was because several environmental variables affected the solubility/volatility and therefore the conversion of the CO_2 concentrations when given in ppm to the mol m^{-3} units required by the flux model.

The DDF optimization relative to z_0 (x_5), α_{AS} (x_6), L_{MO} (x_7), w (x_{11}) and z (x_{12}) was more complicated because fitting the gas flux using an n^{th} order collocation polynomial was only accurate if the n_i steps closely covered the h_i range (for i equal to 5, 6, 7, 11 and 12). This obliges to conjugate h_i with: (1) the chosen x_i units to feed the model, (2) the n_i steps taken and (3) the δ_i size of the steps taken. Therefore, the optimization of the DDF relative to these variables must always be customized to the data set. A good rule of thumb is to choose the units so that h_i has one digit. Afterwards, δ_i should equal the maximum h_i found for all alternative sites divided by n_i keeping in mind that δ_i should never get too big nor too small. In order to illustrate the relevance of such a procedure the optimization of the DDF relative to the depth parametrization was intentionally shown (in Table 1) for a reference site at open ocean ($z = 67$ m) and

OSD
9, 909–975, 2012

an alternative site inside Ria Formosa ($z = 2.5$ m). Big depth differentials may occur in future applications of this DDF tool. Therefore, it was essential to show that the collocation polynomial is so sensitive to depth that $n_i \cdot \delta_i$ must match h_i for the DDF to be accurate. In this case it was 5 1.29 dam =6.45 dam. However, this DDF tool is also intended to be applied to several (possibly many) alternative situations and it is not practical for the user to have to customize δ_i by hand for each new alternative situation. Therefore, the software was updated to do it automatically, whenever required by the user, to whatever variables selected, in whatever units fed to the DDF tool, by setting $\delta_i = h_i / n_i$. With this customization may occur a hidden bias passing undetected. When $n_i \cdot \delta_i$ is very close to h_i the Taylor series always closely matches $f_b - f_a$, irrespective of n_i. This implies that the estimated error (1 minus the sum of all the terms) is very low although each term individually may be biased; in fact, even if relevant higher order terms are missing. The end result is a very low estimated error although the partition of $f_b - f_a$ among the several environmental variables is severely biased. To overcome this problem the choice of Θ_i and n_i must be independent of this customization process where $\delta_i = h_i / n_i$.

One important and immediate application of this DDF tool is to conjugate it with numerical modelling labs such as MOHID, ECO lab, URI's, WRL's or FIO's. These numerical labs simulate the evolution of the physical, chemical and biological properties of the marine and aquatic environments in a particular area. In order to do that the domain area is often divided into thousands to tens of thousands of smaller units. The evolution of the model properties are often estimated at time intervals of a few seconds. It is unfeasible the application of the DDF tool to thousands of locations every few seconds. However, it is possible to drastically lighten it up to the point of enabling this application. The feature that turns the DDF algorithm computationally heavy is the estimation of the hyper-volume of multivariate finite differences needed for the estimation of the partial derivatives. The execution of this calculus for each point and iteration is what makes its application unbearable. The solution to this problem relies on the estimation of this hyper-volume only once for the whole spatial domain over a major

OSD
9, 909–975, 2012

time interval. This hyper-volume must then comprise a grid that, for each of the environmental variables, stretches from the minimum to the maximum recorded values, including reference and all alternative sites. Afterwards, it is possible to accurately estimate the partial derivatives at any point inside this grid because the algorithm used for its estimation (presented in Supplement B) works equally well for k_i being an integer or fractional number. The tests to the estimation of the partial derivatives at any point $x_{i,c}$ inside this grid gave a remarkable accuracy, proving this to be the right solution.

5.4 Insights to the subject system

The gas flux model integrated with the DDF have shown to be valuable tools for the study of any gas crossing the air-water interface, may it be a pollutant or part of a biogeochemical cycle. The gas flux numerical scheme allows to choose the empirical formulations most suited to a particular case or alternatively, mechanistical formulations of broader application. It further allows identifying past cases where inappropriate parametrizations may have been used and quantifying the expected biases. As an example, Oliveira (2012) studied the portuguese coast as a sink/source of CO_2. For that they estimated its flux between the atmosphere and the coastal ocean adjacent to the Douro, Tagus and Sado estuaries. The fluxes were estimated from the formulations by Carini et al. (1996), Raymond and Cole (2001) and Borges et al. (2004b) applied to measures of the required environmental variables. However, actual field measurements of the fluxes were not done, which would enable validation. The problem here was that these formulations were neither developed from open ocean data nor are supported by data on high wind conditions. While the use of the Carini et al. (1996) and Borges et al. (2004b) parametrizations clearly underestimate the flux at open ocean, the extrapolation of the exponential function by Raymond and Cole (2001) is a very wild guess. To ilustrate it, during the cold front that rampant over Europe, the water off-shore Ria Formosa at the 4 February 2012 by 9 h 50 m, was at 15.1 °C, the significant wave heigth was 1.54 m, the wave length was 31.6 m, the average wave period was 4.5 s, the air was at 6 °C and the wind was blowing off-shore at 10 m s^{-1}. Given these

OSD
9, 909–975, 2012

conditions the sea-surface roughness, whitecap and atmospheric instability should play a major role in setting a transfer velocity. The water-side transfer velocities estimated by the Carini et al. (1996) and Borges et al. (2004b) formulations are of 20.3 and 26.8 cm h^{-1}, respectively. When estimated by the Raymond et al. (2000) formulation is of 63.3 cm h^{-1}. When estimated by the AERMOD numerical scheme with the Taylor and Yelland (2001) formulation for roughness length, a Monin-Obukhov length L of −14 m for unstable conditions (arbitrarily, but considering 9 °C difference between water and air) and Zhao et al. (2003) formulations for the effect of wind and whitecap, the water-side transfer velocity is of 71.8 cm h^{-1}; and increases to 86.5 cm h^{-1} if it is used a Monin-Obukhov length L of −10 m.

When using the CO_2 flux across the air-water interface as a proxy for the ecosystem metabolism one must have into account it is also strongly dependent on the influence of turbulence on the transfer velocity. To correct for this Frankignoulle (1988), Smith and Hollibaugh (1993), Raymond et al. (2000), Cole and Caraco (2001), Koné et al. (2009) and Torres et al. (2011) tested using only the difference term of the flux equation. By decomposing the fluxes in all their parcels the DDF further allows accurate estimates of the influence of a wide range of environmental variables in mediating the flux, together with its spatial and temporal variability. Furthermore, this tool allows focusing on the effect of a specific variable at different places, different times or under different methodologies filtering out the undesired effects of changes in other variables. It is also possible to use the DDF tool focusing in a specific aspect. For the subject of the drives for a transfer velocity it only requires replacing the flux by the transfer velocity as the dependent variable. Similarly, for the subject of the drives for a difference between the gas concentrations in the air and water phases it only requires the replacement of the flux by the ΔC or Δppm as the dependent variables.

The gains brought by this new gas flux numerical model and DDF tool were clearly demonstrated with the comparison between Ria Formosa at the 14 of April 2011 and its surrounding coastal ocean at the 3 March 2011. While the coastal ocean was behaving autotrophically the Ria Formosa was behaving heterotrophically, at least between 11 h

OSD
9, 909–975, 2012

and 13 h and at that particular site. The bulk of the CO_2 flux difference was indeed due to the difference in the CO_2 concentrations in the water inside and outside. However, there were also other factors taking part that the DDF enabled to set aside. While the transfer velocity in the ocean was set by turbulence from above, inside the mesotidal lagoonary system it was set majorly by turbulence from below. A similar contrast was presented by Borges et al. (2004a) when comparing between micro, meso and macrotidal estuaries. On the other hand, Ho et al. (2011) determined the transfer velocity in the Hudson river was basically set by wind speed and independent of current drag with the bottom. Still, these authors admitted such results may have been influenced by samples having been taken tendentiously over ≥ 5 m depths.

The ΔCO_2 series suggest Ria Formosa could be behaving autotrophically at the early March when the water was around 17 °C and could be behaving heterotrophically at the mid April when the water was around 20.5 °C. This change with temperature may be related to the dominant biological process taking place. Photosynthesis by seagrass meadows is much less sensitive to temperature changes than respiration by bacteria. A seasonal shift of the CO_2 balance in estuaries, lagoonary systems and coastal waters was already reported by Raymond et al. (2000), Cole and Caraco (2001), Borges (2005), Koné et al. (2009), Hunt et al. (2011), Oliveira (2012). The water column at the sampled Ria Formosa channel during ebb tide changed from autotrophic to heterotrophic in a couple of hours. It proves there was a strong spatial/temporal heterogeneity in the CO_2 balance. This was already found for estuaries, lagoonary systems and coastal waters by Raymond et al. (2000), Cole and Caraco (2001), Frankignoulle et al. (2001), Borges et al. (2004a), Koné et al. (2009), Hunt et al. (2011), Torres et al. (2011), Oliveira (2012). In the present case it is hypothesized whether the metabolic status of a particular section of the water column was related to it being over a seagrass meadow or a mud-flat in its near past.

OSD
9, 909–975, 2012

6 Conclusions

Wide spatial and temporal variabilities of gas concentrations in the water, in the overlying air and their fluxes across the air-water interface are widely documented for the open oceans, the coastal oceans and riverine systems. These gas fluxes have a multitude of potential forcing functions. However, their integration and the establishment of their relative importances has been underachieved. This is particularly evident from how atmospheric stability and sea-surface roughness have been devoted to oblivion in studies about riverine systems and coastal waters, or how turbulence from current drag with the bottom is often forgotten in these same studies. The currently presented numerical tools give a significant contribution to this subject. Now it is easier to use a single model for any type of marine and freshwater environment and to conclude the differences found between those report exclusively to the environments and not to different numerical options. Furthermore, the numerical scheme allows for the upgrade of each relevant environmental process already implemented as well as the addition of new processes. Any interested researcher is free to add a particular formulation for its own personal use and is further invited to share it with everyone else. The versatility of the present model, tools and software allows the user to follow two distinct approaches. The user may choose to use the formulations available in the literature that best fit to a particular situation. These tend to be more of an empirical nature and to fail under largely different environmental conditions. Alternatively, the user may build the model upon a more mechanistic approach, computationally heavier, but tending to yield better global fits. The DDF tool allows for the quantification of the effects of all the environmental variables and processes involved in the gas flux across a particular air-water interface relative to a reference one. It further allows to focus in a specific variable or process eliminating the error from the remaining ones.

Supplementary material related to this article is available online at: http://www.ocean-sci-discuss.net/9/909/2012/osd-9-909-2012-supplement.zip.

OSD
9, 909–975, 2012

Acknowledgements. To Martin Johnson, Marcos Mateus, Flávio Martins and Oscar Ferreira for their comments and insights and to the ALGAE group for the support and participation in the field surveys.

Vasco Vieira was supported by a *Fundação para a Ciência e Tecnologia* (FCT) grant PTDC/AAC-CLI/103348/2008.

References

Borges, A. V.: Do we have enough pieces of the jigsaw to integrate CO2 fluxes in the coastal ocean? Estuaries, 28, 3–27, 2005. 911, 948

Borges, A. V., Delille, B., Schiettecatte, L. S., Gazeau, F., Abril, G., and Frankignoulle, M.: Gas transfer velocities of CO2 in three European estuaries (Randers Fjord, Scheldt, and Thames), Limnol. Oceanogr., 49, 1630–1641, 2004a. 913, 914, 919, 948

Borges, A. V., Vanderborght, J. P., Schiettecatte, L. S., Gazeau, F., Ferron-Smith, S., Delille, B., and Frankignoulle, M.: Variability of the Gas Transfer Velocity of CO2 in a Macrotidal Estuary (the Scheldt), Estuaries, 27, 593–603, 2004b. 912, 913, 914, 915, 918, 930, 938, 946, 947

Borges, A. V., Delille, B., and Frankignoulle, M.: Budgeting sinks and sources of CO2 in the coastal ocean: Diversity of ecosystems counts, Geophys. Res. Lett., 32, L14601, doi:10.1029/2005GL023053, 2005. 911

Capps, S. B. and Zender, C. S.: Global ocean wind power sensitivity to surface layer stability, Geophys. Res. Lett., 36, L09801, doi:10.1029/2008GL037063, 2009. 921

Carini, S., Weston, N., Hopkinson, C., Tucker, J., Giblin, A., and Vallino, J.: Gas exchange rates in the Parker River estuary, Massachusetts. Biol. Bull., 191, 333–334, 1996. 910, 911, 914, 915, 918, 919, 930, 938, 946, 947

Charnock, H.: Wind stress on a water surface, Quart. J. Roy. Meteor. Soc., 81, 639–640, 1955. 942

Chelton, D. B. and Freilich, M. H.: Scatterometer-based assessment of 10-m wind analyses from the operational ECMWF and NCEP numerical weather prediction models, Mon. Weather. Rev., 133, 409–429, 2005. 921

Cole, J. J. and Caraco, N. F.: Carbon in catchments: connecting terrestrial carbon losses with aquatic metabolism, Mar. Freshwater Res., 52, 101–110, 2001. 911, 913, 947, 948

Donelan, M. A.: The dependence of the aerodynamic drag coefficient on wave parameters,

First International, Conference on Meteorology and Air-Sea Interaction of the Coastal Zone, The Hague, Netherlands, Amer. Meteor. Soc., 381–387, 1982. 922
Donelan, M. A.: Air-sea interaction, in: Ocean Engineering Science, vol.9, The Sea, edited by: Le Mehaute, B. and Hanes, D. M., John Wiley, Hoboken, N. J., 239–292. 1990. 922
Duan, Z. and Martin, J. L.: Integration of impact factors of gas-liquid transfer rate, 37th Annual Mississippi Water Resources Conference, http://www.wrri.msstate.edu/pdf/duan07.pdf, last access: 2011, 2007. 914, 943
Duarte, C. M. and Prairie, Y. T.: Prevalence of heterotrophy and atmospheric CO2 emissions from aquatic ecosystems, Ecosystems, 8, 862–870, 2005. 911
Duce, R. A., Liss, P. S., Merrill, J. T., Atlas, E. L., Buat-Menard, P., Hicks, B. B., Miller, J. M., Prospero, J. M., Arimoto, R., Church, T. M., Ellis, W., Galloway, J. N., Hansen, L., Jickells, T. D., Knap, A. H., Reinhardt, K. H., Schneider, B., Soudine, A., Tokos, J. J., Tsunogai, S., Wollast, R., and Zhou, M.: The Atmospheric Input of Trace Species to the World Ocean, Global Biogeochem. Cy., 5, 193–259, 1991. 917, 919, 929, 930
Fairall, C. W., Bradley, E. F., Rogers, D. P., Edson, J. B., and Young, G. S.: Bulk parameterization of air-sea fluxes for tropical ocean global atmosphere coupled ocean atmosphere response experiment, J. Geophys. Res., 101, 3747–3764, 1996. 916
Fairall, C. W., Hare, J. E., Edson, J. B., and McGillis, W.: Parameterization and micrometeorological measurement of air-sea gas transfer, Bound. Lay. Meteorol., 96, 63–106, 2000. 915
Fairall, C. W., Bradley, E. F., Hare, J. E., Grachev, A. A., and Edson, J. B.: Bulk parameterization of air-sea fluxes: updates and verification for the COARE algorithm, J. Climate, 16, 571–591, 2003. 914, 916, 921, 922, 929, 939, 942
Frankignoulle, M.: Field measurements of air-sea CO2 exchange, Limnol. Oceanogr., 33, 313–322, 1988. 910, 913, 918, 947
Frankignoulle, M. and Borges, A. V.: European continental shelf as a significant sink for atmospheric CO2, Global Biogeochem. Cy., 15, 569–576, 2001. 910
Frankignoulle, M., Borges, A., and Biondo, R.: A new design of equilibrator to monitor carbon dioxide in highly dynamic and turbid environments, Wat. Res., 35, 1344–1347, 2001. 948
Frew, N. M., Bock, E. J., Schimpf, U., Hara, T., Haubecker, H., Edson, J. B., McGillis, W. R., Nelson, R. K., McKenna, S. P., Uz, B. M., and Jahne, B.: Air-sea gas transfer: Its dependence on wind stress, small-scale roughness, and surface films, J. Geophys. Res., 109: C08S17, doi:10.1029/2003JC002131, 2004. 914, 916, 939, 941, 942, 943

OSD
9, 909–975, 2012

Grachev, A. A. and Fairall, C. W.: Dependence of the MoninObukhov Stability Parameter on the Bulk Richardson Number over the Ocean, J. Appl. Meteorol., 36, 406–414, 1997. 916, 921, 929, 942
Hayduk, W. and Laudie, H.: Prediction of diffusion coefficients for non-electrolytes in dilute aqueous solutions, AIChE Journal, 20, 611–615, 1974. 915, 919
Hayduk, W. and Minhas, B. S.: Correlations for prediction of molecular diffusivities in liquids, Can. J. Chem. Eng., 60, 295–299, 1982. 915, 919
Ho, D. T., Zappa, C. J., McGillis, W. R., Bliven, L. F., Ward, B., Dacey, J. W. H., Schlosser, P., and Hendricks, M. B.: Influence of rain on air-sea gas exchange: Lessons from a model ocean, J. Geophys. Res., 109, doi:10.1029/2003JC001806, 2004. 914
Ho, D. T., Schlosser, P., and Philip, M. O.: On factors controlling air-water gas exchange in a large tidal river, Estuar. Coast., 34, 1103–1116, 2011. 948
Hoffman, R. N. and Leidner, S. M.: An introduction to the near-realtime QuikSCAT data, Weather Forecast., 20, 476–493, 2005. 921
Hunt, C. W., Salisbury, J. E., Vandemark, D., and McGillis, W.: Contrasting Carbon Dioxide Inputs and Exchange in Three Adjacent New England Estuaries, Estuar. Coast., 34, 68–77, 2011. 910, 913, 948
Hwang, P. A.: Wave number spectrum and mean square slope of intermediate-scale ocean surface waves, J. Geophys. Res., 110: C10029, doi:10.1029/2005JC003002, 2005. 942
Jeffery, C., Robinson, I., and Woolf, D.: Tuning a physically-based model of the air-sea gas transfer velocity, Ocean Modell., 31, 28–35, doi:10.1016/j.ocemod.2009.09.001, 2010. 929
Johnson, M. T.: A numerical scheme to calculate temperature and salinity dependent air-water transfer velocities for any gas, Ocean Sci., 6, 913–932, 2010, http://www.ocean-sci.net/6/913/2010/. 911, 913, 915, 916, 917, 918, 919, 923, 929, 930, 937, 938
Koné, Y. J. M., Abril, G., Kouadio, K. N., Delille, B., and Borges, A. V.: Seasonal Variability of Carbon Dioxide in the Rivers and Lagoons of Ivory Coast (West Africa), Estuar. Coast., 32, 246–260, 2009. 911, 913, 947, 948
Lange, B., Larsen, S., Hjstrup, J., and Barthelmie, R.: Importance of thermal effects and sea surface roughness for offshore wind resource assessment, J. Wind Eng. Ind. Aerod., 92, 959–988, 2004. 921, 942
Liss, P.: Processes of gas exchange across an air-water interface, Deep-Sea Res. Oceanogr. Abstracts, 20, 221–238, 1973. 917, 919

OSD
9, 909–975, 2012

Liss, P. S. and Slater, P. G.: Flux of gases across the air-sea interface, Nature, 247, 181–184, 1974. 916

Liss, P. S. and Merlivat, L.: Air-sea gas exchange rates: Introduction and synthesis, in: The role of sea-air exchange in geochemical cycling, edited by: Buat-Menard, P., D. Riedel, Hinghan, MA, 113–139, 1986. 914, 918

Mackay, D. and Yeun, A. T. K.: Mass transfer coefficient correlations for volatilization of organic solutes from water, Environ. Sci. Technol., 17, 211–217, 1983. 911, 913, 914, 916, 917, 918, 919, 929, 930, 932, 933, 937, 940

McGillis, W. R., Edson, J. B., Ware, J. D., Dacey, J. W. H., Hare, J. E., Fairall, C. W., and Wanninkhof. R.: Carbon dioxide flux techniques performed during GasEx 98, Mar. Chem., 75, 267–280, 2001. 914, 918, 930

Mears, C. A., Smith, D. K., and Wentz, F. J.: Comparison of Special Sensor Microwave Imager and buoy-measured wind speeds from 1987 to 1997, J. Geophys. Res., 106, 719–729, 2001. 921

Memery, L. and Merlivat, L.: Modelling of gas flux through bubbles at the air water Interface, Tellus, 37, 272–285, 1985. 914, 938, 940, 941

Moon, I., Ginis, I., and Hara, T.: Effect of surface waves on Charnock coefficient under tropical cyclones, Geophys. Res. Lett., 31, L20302,doi:10.1029/2004GL020988, 2004. 939, 942

Nightingale, P. D., Malin, G., Law, C. S., Watson, A. J., Liss, P. S., Liddicoat, M. I., Boutin J., and Upstill-Goddard, R. C.: In Situ evaluation of air-sea gas exchange parameterizations using novel conservative and volatile tracers, Global Biogeochem. Cy., 14, 373–387, 2000. 914, 918

O'Connor, D. and Dobbins, W.: Mechanisms of reaeration in natural streams, T. Am. Soc. Civ. Eng., 123, 641–684, 1958. 912, 915, 919, 931

Oliveira, A. P. E.: Fluxos de CO2 na interface ar gua num sistema estuarino portuguls e zona costeira adjacente. PhD. Instituto Superior Tcnico, Universidade Tcnica de Lisboa, Portugal, 2011. 910

Oliveira, A. P., Cabeçadas, G., and Pilar-Fonseca, T.: Iberia Coastal Ocean in the CO2 Sink/Source Context: Portugal Case Study, J. Coast. Res., 28, 184–195, 2012. 911, 946, 948

Oost, W. A., Komen, G. J., Jacobs, C. M. J., and van Oort, C.:, New evidence for a relation between wind stress and wave age from measurements during ASGAMAGE, Bound. Lay. Meteorol., 103, 409–438, 2002. 914, 922

OSD

9, 909–975, 2012

Raymond, P. A. and Cole, J. J.: Gas Exchange in Rivers and Estuaries: Choosing a Gas Transfer Velocity, Estuaries, 24, 312–317, 2001. 911, 914, 915, 918, 919, 930, 938, 946
Raymond, P. A., Bauer J. E., and Cole. J. J.: Atmospheric CO2 evasion, dissolved inorganic carbon production, and net heterotrophy in the York River estuary, Limnol. Oceanogr, 45, 1707–1717, 2000. 910, 913, 947, 948
Sander, R.: Compilation of Henry's law constants for inorganic and organic species of potential importance in environmentalcChemistry (Version 3), http://www.henrys-law.org, last access: 2011, 1999. 913, 918, 923, 937
Sethuraman, S. and Raynor, G. S.: Surface drag coefficient dependence on the aerodynamic roughness of the sea, J. Geophys. Res., 80, 4983–4988, 1975. 917, 937, 939, 940, 942
Sethuraman, S. and Brown, R. M.: Validity of the log-linear profile relationship over a rough terrain during stable conditions, Bound-Lay. Meteorol., 10, 489–501, 1976. 920, 922, 933, 942
Shahin, U. M., Holsen, T., and Odabasi, M.: Dry deposition measured with a water surface sampler: a comparison to modeled results, Atmos. Environ., 36, 3267–3276, 2002. 917, 919, 929
Sidinei, M. T., Enrich-Prast, A., Gonalves Jr., J. F., dos Santos, A. M., and Esteves, F. A.: Metabolism and gaseous exchanges in two coastal lagoons from Rio de Janeiro with distinct limnological characteristics, Braz. Arch. Biol. Tech., 44, 433–438, 2001. 911
Smith, S. D.: Wind stress and heat flux over the ocean in gale force winds, J. Phys. Oceanogr., 10, 709–726, 1980. 917, 919, 929, 930, 937
Smith, S. D., Anderson, R. J., Oost, W. A., Kraan, C., Maat, N., DeCosmo, J., Katsaros, K. B., Davidson, K. L., Bumke, K., Hasse, L., and Chadwick, H. M.: Sea surface wind stress and drag coefficients: The HEXOS results, Bound. Lay. Meteorol., 60, 109–142, 1992. 922, 937
Smith, S. V. and Hollibaugh, J. T.: Coastal metabolism and the oceanic organic carbon balance, Rev. Geophys., 31, 75–89, 1993. 911, 947
Sweeney, C.: The annual cycle of surface CO2 and O2 in the Ross Sea: A model for gas exchange on the continental shelves of Antarctica, in: Biogeochemistry of the Ross Sea, edited by: DiTullio, G.R. and Dunbar, R. B., Antar. Res. S., vol 78, AGU, Washington, D.C., 295–312, 2003. 910
Sweeney, C., Gloor, E., Jacobson, A. R., Key, R. M., McKinley, G., Sarmiento, J. L., and Wanninkhof, R.: Constraining global air-sea gas exchange for CO2 with recent bomb 14C measurements, Global Biogeochem. Cy., 21: GB2015, doi:200710.1029/2006GB002784, 2007.

OSD
9, 909–975, 2012

914, 918
Takahashi, T., Sutherland, S. C., Sweeney, C., Poisson, A., Metzl, N., Tilbrook, B., Bates, N., Wanninkhof, R., Feely, R. A., Sabine, C., and Olafsson, J.: Biological and temperature effects on seasonal changes of pCO2 in global surface ocean, Deep-Sea Res., 49, 1601–1622, 2002. 910
Takahashi, T., Sutherland, S. C., Wanninkhof, R., Sweeney, C., Feely, R. A., Chipman, D. W., Hales, B., Friederich, G., Chavez, F., Watson, A., Bakker, D. C. E., Schuster, U., Metzl, N., Yoshikawa-Inoue, H., Ishii, M., Midorikawa, T., Sabine, C., Hopemma, M., Olafsson, J., Arnarson, T. S., Tilbrook, B., Johannessen, T., Olsen, A., Bellerby, R., de Baar, H. J. W., Nojiri, Y., Wong C. S., and Delille, B.: Climatological mean and decadal change in surface ocean pCO2, and net sea-air CO2 flux over the global oceans, Deep-Sea Res., 56, 554–577, doi:10.1016/j.dsr2.2008.12.009, 2009. 910
Taylor, P. K. and Yelland, M. J.: The dependence of sea surface roughness on the height and steepness of the waves, J. Phys. Oceanogr., 31, 572–590, 2001. 914, 917, 919, 922, 932, 937, 939, 940, 942, 947
Torres, R., Pantoja, S., Harada, N., González, H. E., Daneri, G., Frangopulos, M., Rutllant, J. A., Duarte, C. M., Rúiz-Halpern, S., Mayol, E., and Fukasawa, M.: Air-sea CO_2 fluxes along the coast of Chile: From CO_2 outgassing in central northern upwelling waters to CO_2 uptake in southern Patagonian fjords, J. Geophys. Res., 116, C09006, doi:10.1029/2010JC006344, 2011. 947, 948
Turk, D., Zappa, C. J., Meinen, C. S., Christian, J. R., Ho, D. T., Dickson, A. G., and McGillis, W. R.: Rain impacts on CO2 exchange in the western equatorial Pacific Ocean, Geophys. Res. Lett., 37, L23610, doi:10.1029/2010GL045520, 2010. 913, 914
Upstill-Goddard, R. C.: Air-sea gas exchange in the coastal zone, Estuar. Coast. Shelf S., 70, 388–404, 2006. 913, 937, 941
Vandemark, D., Salisbury, J. E., Hunt, C. W., Shellito, S. M., Irish, J. D., McGillis, W. R., Sabine, C. L., and Maenner, S. M.: Temporal and spatial dynamics of CO2 air sea flux in the Gulf of Maine, J. Geophys. Res., 116: C01012, doi:10.1029/2010JC006408, 2011. 910, 913
Vickers, D. and Mahrt, L.: Evaluation of the air-sea bulk formula and sea-surface temperature variability, J. Geophys. Res., 111, 5002–5016, 2006. 932, 940
Wanninkhof, R.: Relationship between wind speed and gas exchange over the ocean, J. Geophys. Res., 97, 7373–7382, 1992. 913, 914, 915, 918
Wilke, C. R. and Chang, P.: Correlation of diffusion coefficients in dilute solutions, AIChE Jour-

OSD
9, 909–975, 2012

nal, 1, 264–270, 1955. 915, 919
Woodward, J. L.: Estimating the flammable mass of a vapor cloud. Center for Chemical Process Safety/American Iintitute of Chemical Engineers, New York, NY, 296 pp., 1998. 920, 922, 933
Woolf, D. K.: Bubbles and their role in gas exchange, in: The Sea Surface and Global Change, edited by: Liss, P. S. and Duce, R. A., Cambridge University Press, Cambridge, 173–205, 1997. 914
Woolf, D. K.: Parameterization of gas transfer velocities and sea-state-dependent wave breaking, Tellus, 57B, 87–94, 2005. 914, 915, 940
Zappa, C. J., McGillis, W. R., Raymond, P. A., Edson, J. B., Hintsa, E. J., Zemmelink, H. J. Dacey, J. W. H., and Ho, D. T.: Scaling gas transfer with turbulent dissipation for a range of environmental processes, Geophys. Res. Lett., 34: L10601, doi:10.1029/2006GL028790, 2007. 913, 914
Zappa, C. J., Ho, D. T., McGillis, W. R., Banner, M. L., Dacey, J. W. H., Bliven, L. F., Ma, B., and Nystuen, J.: Rain-induced turbulence and air-sea gas transfer, J. Geophys. Res., 114, C07009, doi:10.1029/2008JC005008, 2009. 914
Zhao, D. and Xie, L.: A practical bi-parameter formula of gas transfer velocity depending on wave states, J. Oceanogr., 66, 663–671, 2010. 914
Zhao, D., Toba, Y., Suzuki, Y., and Komori, S.: Effect of wind waves on air-sea gas exchange: proposal of an overall CO2 transfer velocity formula as a function of breaking-wave parameter, Tellus B, 55, 478–487, 2003. 912, 913, 914, 917, 918, 931, 933, 940, 947

OSD
9, 909–975, 2012

Table 1. Optimization of the DDF. (a) any D_w scheme, (b) with whitecap formulation. (ad. fit.) δ_i adjusted to fit h_i. Optimality is **bolded**.

x_i	Θ	n	Error(%)	Further options	$[CO_2]$units
C_a	**1**	**1**;5	10^{-12};10^{-11}		ppm
C_a	**1**	**1**	10^{-14}		mol m^{-3}
T_a	1;**2**;3;4;5	1;**2**;3;4;5	3.876;**0.285**;0.133;0.138;0.138	k_a:Joh10	ppm
T_a	1;**2**;3;4;5	1;**2**;3;4;5	3.877;**0.285**;0.133;0.138;0.138	k_a:Joh10(COARE)	ppm
T_a	1;**2**;3;4;5	1;**2**;3;4;5	3.881;**0.286**;0.133;0.138;0.138	k_a:M&Y83	ppm
T_a	1;2;3;**4**;5	1;2;3;**4**;5	83.36;12.80;1.337;**0.023**;10^{-4}	k_a:M&Y83	mol m^{-3}
P	**1**;2;3	**1**;2;3	**0.138**;0.138;0.138		ppm
P	**1**;2;3	**1**;2;3	**0.046**;10^{-4};10^{-6}		mol m^{-3}
u_{10}	1;2;**3**;4;5	1;2;**3**;4;5	48.5;8.9;**0.04**;0.05;0.04	k_w:McG01	ppm
u_{10}	1;2;**3**;4;5	5	53.3;13.2;**0.17**;0.10;0.04	k_w:McG01	ppm
u_{10}	1;2;**3**;4;5	1;2;**3**;4;5	48.5;8.9;**0.07**;0.01;0.001	k_w:McG01	mol m^{-3}
u_{10}	1;2;**3**;4;5	1;2;3;4;5	32.7;6.89;**0.94**;0.12;0.04	k_w:R&C01	ppm
u_{10}	1;2;3;**4**;5	5	35.8;9.46;1.83;**0.39**;0.04	k_w:R&C01	ppm
u_{10}	**1**;2;3;4;5	**1**;2;3;4;5	0.07;0.034;0.036;0.037;0.037	k_w:Bea04	ppm
u_{10}	**1**;2;3;4;5	5	**0.07**;0.033;0.036;0.038;0.037	k_w:Bea04	ppm
z_0	1;2;3;4;5	1;2;3;4;5	67.9;56.3;49.1;43.7;39.2	δ=1;z_0 =mm	ppm
z_0	**1**;2;3;4;5	**1**;2;3;4;5	0.138	δ=ad. fit. z_0 =mm	ppm
α_{AS}	1;2;3;4;**5**	1;2;3;4;**5**	100;99;98;97;**0.138**	δ=1	ppm
α_{AS}	**1**	**1**	**0.138**	δ=ad. fit.	ppm
L_{MO}	1; 5	1; 5	303; 661	δ=1	ppm
L_{MO}	**1**	**1**	**0.138**	δ=ad. fit.	ppm
C_w	**1**;2;5	**1**;2;3;4;5	**0.015**		ppm
C_w	**1**	**1**	10^{-14}		mol m^{-3}
S	1;2;3;4;5	5	0.269;0.037;0.037;0.037;0.037	α:Joh10 (a)	ppm
S	1;2;3;4;5	5	0.355;0.038;0.037;0.037;0.037	α:Bea04	ppm
S	**1**;2;3;4;5	**1**;2;3;4;5	**0.037**;0.037;0.037;0.037;0.037	α:both (a)	ppm
S	**1**;2;3;4;5	**5**	**0.42**;0.0005;10^{-7};10^{-10};10^{-14}	α:Joh10 (a)	mol m^{-3}
S	**1**;2;3;4;5	5	**0.42**;0.0012;10^{-6};10^{-9};10^{-14}	α:Bea04	mol m^{-3}
S	**1**;2;3;4;5	**1**;2;3;4;5	**0**;0;0;0;10^{-14}	α:both(a)	mol m^{-3}
w	1;2;3;4;5	1;2;3;4;5	44.9;31;24;19.7;16.7	δ=1 w = m min^{-1}	ppm
w	1;2;3;4;5	1;2;3;4;5	44.6;30.5;23.4;19;15.8	δ=1 w = hm h^{-1}	ppm
w	1;2;3;4;**5**	1;2;3;4;**5**	3.66;3.01;2.55;2.2;**1.92**	δ=ad. fit. w = hm h^{-1}	ppm
z	1;2;3;4;5	1;2;3;4;5	341;612;615;341;91.6	$delta$=1 z=m	ppm
z	1;2;3;4;**5**	1;2;3;4;**5**	269;338;201;46.5;**0.04**	δ=ad. fit. z =m	ppm

OSD
9, 909–975, 2012

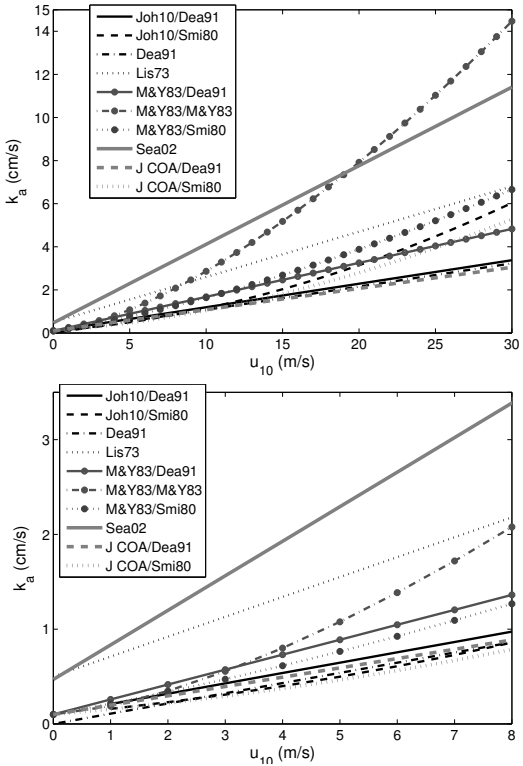

Fig. 1. Effect of wind (u_{10}) below 30 m s^{-1} (up) and below 5 m s^{-1} (down) on the air-side transfer velocity (k_a). First reference: friction velocity equation. Second reference: drag coefficient equation. 'Joh10': Johnson (2010); 'Dea91': Duce et al (1991); 'Lis73': Liss (1973); 'M&Y83': Mackay and Yeun (1983); 'Sea02': Shahin et al 2002; 'J COA': Johnson (2010) adaptation of COARE; 'Smi80': Smith (1980).

OSD
9, 909–975, 2012

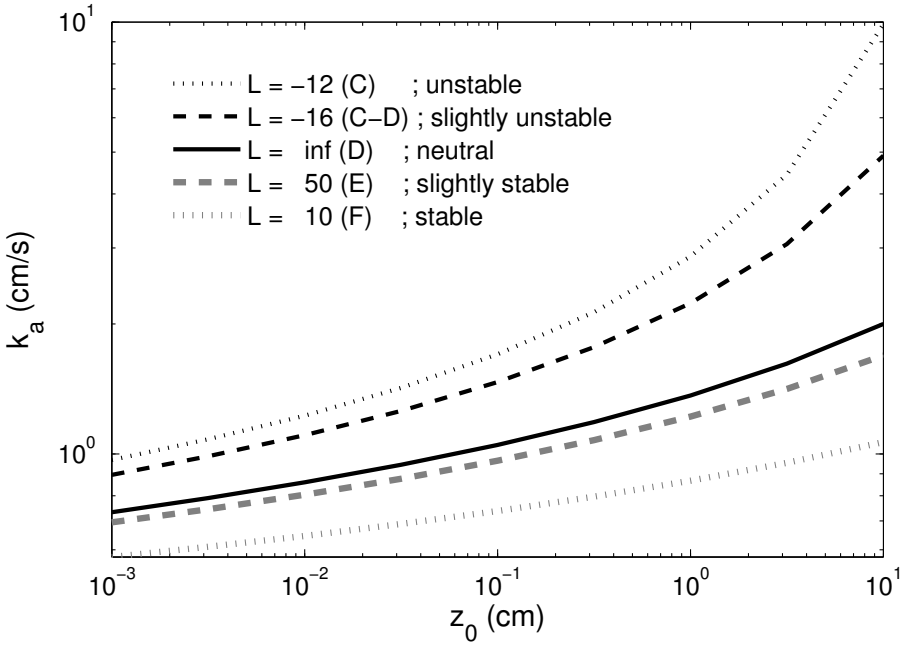

Fig. 2. Effects of surface roughness (z_0) and atmospheric stability (Monin-Obukhov length L) in the air-side transfer velocity (k_a). Within brackets are the Pasquill-Gifford stability classes. Wind at $u_{10} = 5\,\mathrm{m\,s^{-1}}$, k_a by Mackay and Yeun (1983) and atmospheric stability $\alpha = 4.5$.

OSD
9, 909–975, 2012

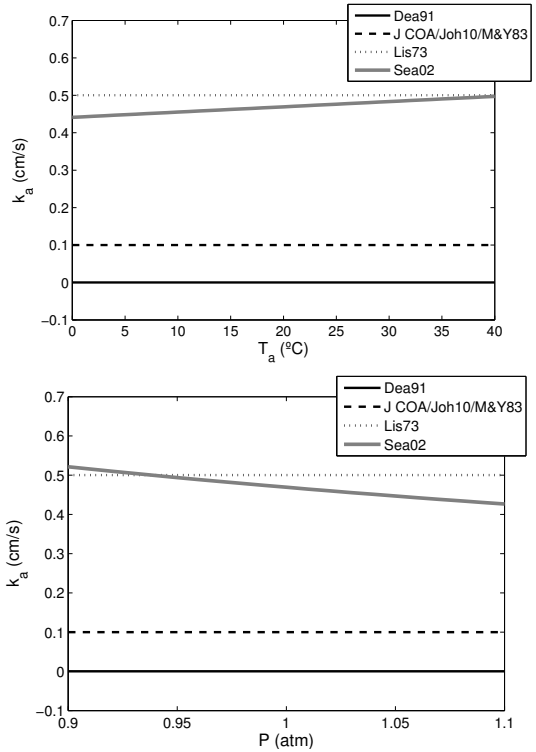

Fig. 3. Effects of T_a (up) and P (down) on the air transfer velocity. 'Joh10': Johnson (2010); 'Dea91': Duce et al (1991); 'Lis73': Liss (1973); 'M&Y83': Mackay and Yeun (1983); 'Sea02': Shahin et al 2002; 'J COA': Johnson (2010) adaptation of COARE. Drag Coefficient estimated from Smith (1980).

OSD
9, 909–975, 2012

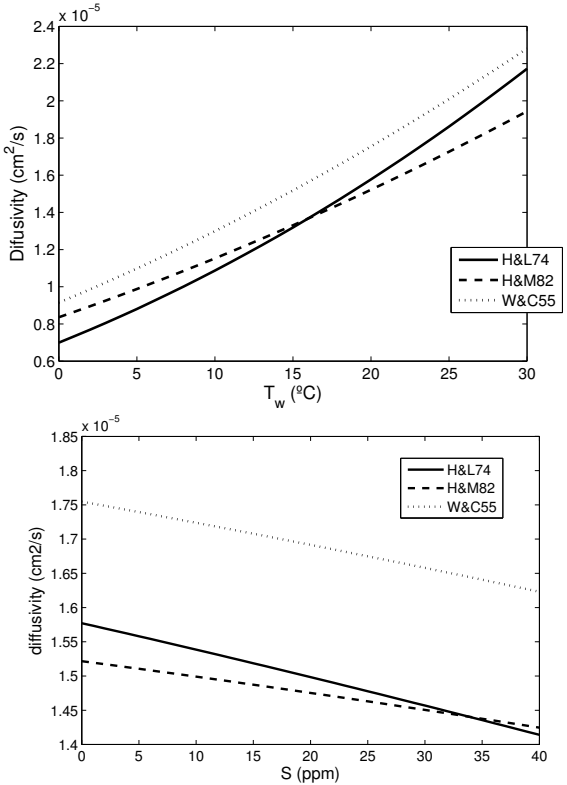

Fig. 4. Effects of T_w (up) and S (down) on the water diffusivity. 'H&L74': Hayduk and Laudie (1974); 'H&M82': Hayduk and Minhas (1982); 'W&C55': Wilkie and Chang (1955).

OSD
9, 909–975, 2012

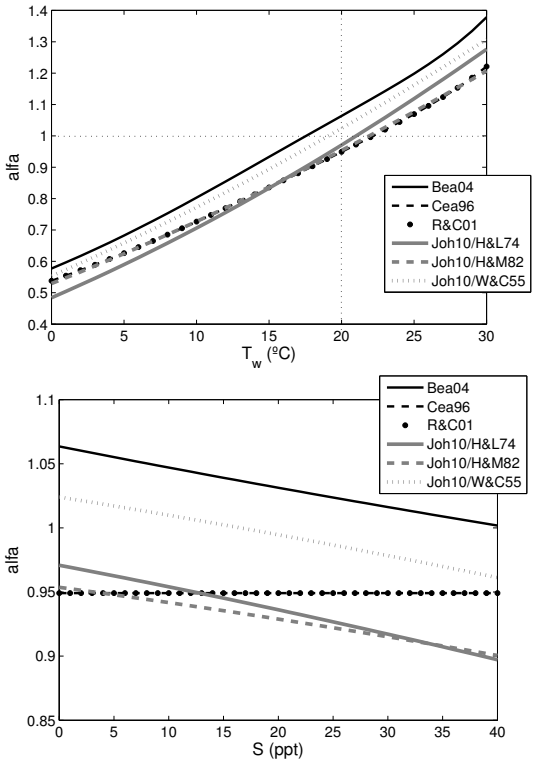

Fig. 5. Effects of T_w (up) and S (down) on the chemical enhancement factor (α) in fresh water. 'Bea04': Borges et al (2004); 'Cea96': Carini et al (1996); 'R&C01' : Raymond and Cole 2001. Johnson (2010) α estimate with water diffusivity by: 'H&L74': Hayduk and Laudie (1974); 'H&M82': Hayduk and Minhas (1982); 'W&C55': Wilkie and Chang (1955).

OSD
9, 909–975, 2012

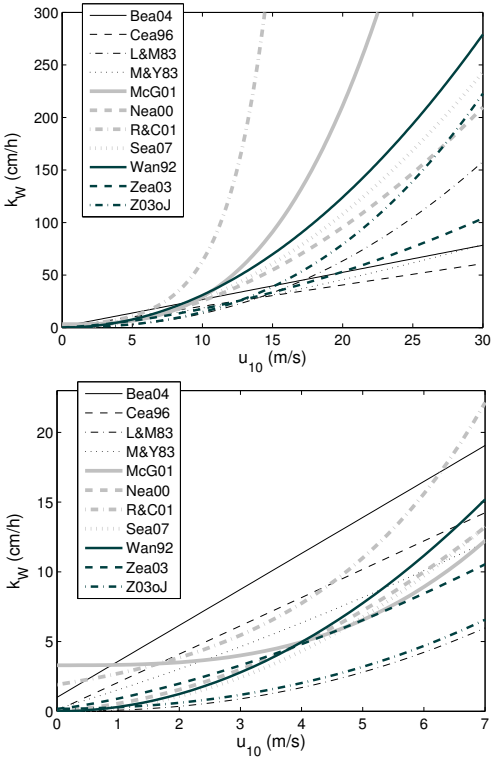

Fig. 6. Effect of u_{10} below 30 m s^{-1} (up) and below 7 m s^{-1} (down) on the water transfer velocity (k_w^{wind}). 'Bea04': Borges et al., (2004); 'Cea96': Carini et al (1996); 'R&C01': Raymond and Cole (2001); 'L&M83': Liss and Merlivat (1983); 'M&Y83': Mackay andYeun (1983); 'McG01': McGillis (2001); 'Nea00': Nightingale et al., (2000); 'Sea07': Shahin et al., (2007); 'Wan9': Wanninkhof (1992); 'Zea03': Zhao et al., (2003, not accounting for whitecap); 'Z03oJ': Zhao et al., (2003) on data from Jähne et al., (1985). Where applicable the u_* was estimated from u_{10} using the drag coefficient by Smith (1980).

OSD
9, 909–975, 2012

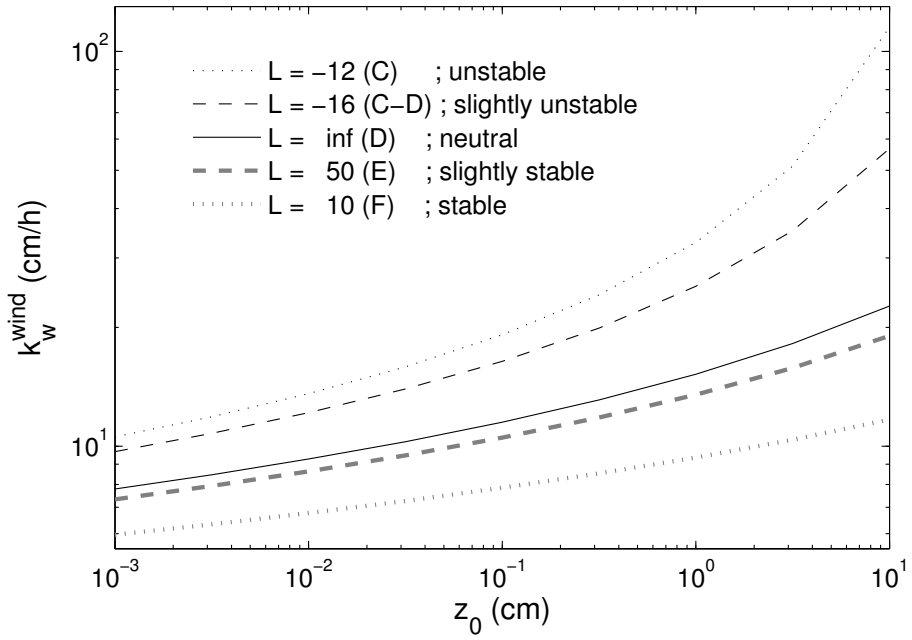

Fig. 7. Effect of surface roughness (measured by z_0) and atmospheric stability (measured by Monin-Obukhov length L) in the water-side transfer velocity (k_w). Within brackets are the Pasquill-Gifford stability classes. $u_{10} = 5\,m\,s^{-1}$, k_w^{wind} by Zhao et al., (2003), chemical enhancement factor α by Johnson (2010), D_w by Wilkie and Chang (1955) and atmospheric stability α=4.5.

OSD
9, 909–975, 2012

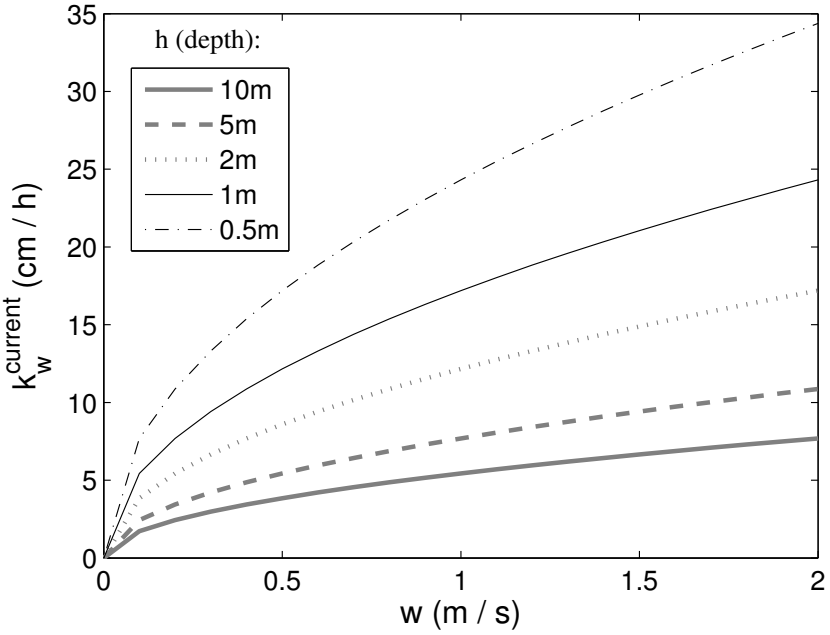

Fig. 8. Effect of water current (w) and depth (h) on the water transfer velocity ($k_w^{current}$) according to O'Connor and Dobbins (1958).

OSD
9, 909–975, 2012

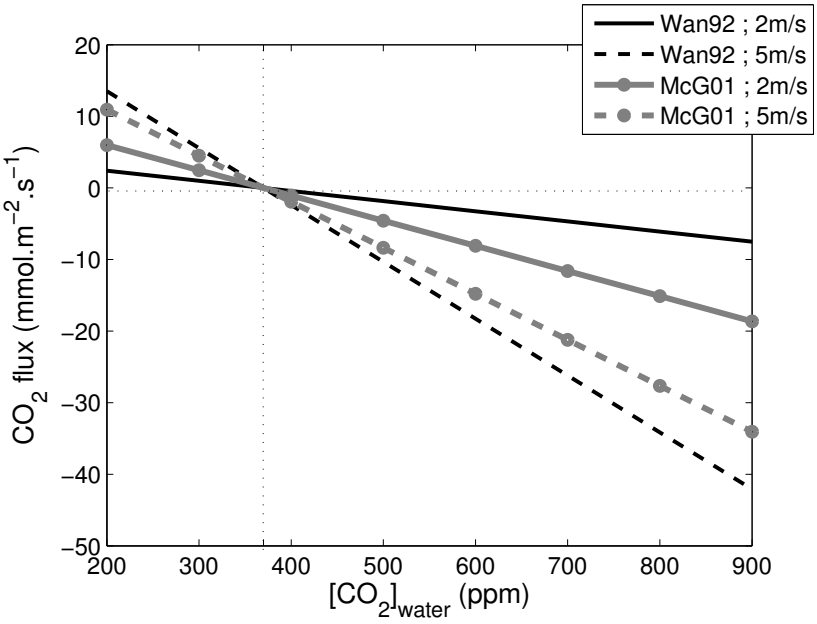

Fig. 9. Effects of $[CO_2]_w$ and u_{10} in the CO_2 flux across the air-water interface. Transfer velocity by double layer (DL), k_w by Wanninkhof 1992 ('Wan92') or McGillis 2001('McG01'), with α by Johnson 2010, water diffusivity by Wilkie and Chang (1955), air drag coefficient by Smith (1980) and k_a by Mackay and Yeun (1983).

OSD
9, 909–975, 2012

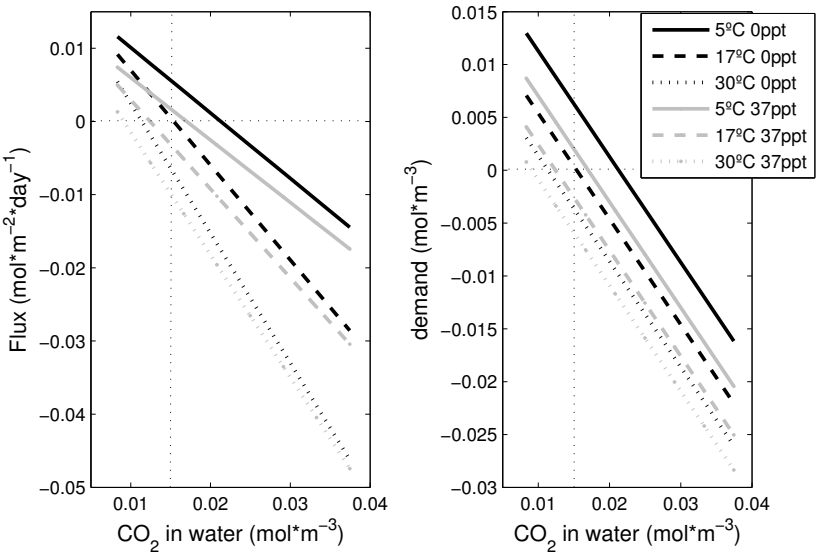

Fig. 10. Effects of $[CO_2]_w$, T_w and S in the CO_2 flux across the air-water interface (left) and in the ΔCO_2 (right). Environmental reference situation changed to 0.1 m s^{-1} wind and 0.1 m s^{-1} current. Transfer velocity (k) by double layer (DL), k_w^{wind} by McGillis (2001), α by Johnson (2010), D_w by Wilkie and Chang (1955), CD by Smith (1980) and k_a by Mackay and Yeun (1983).

OSD
9, 909–975, 2012

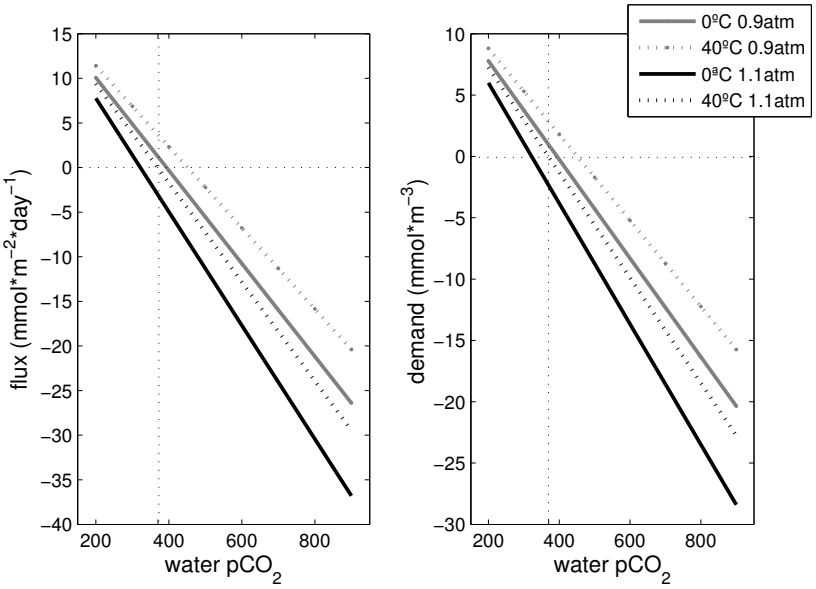

Fig. 11. Effects of the $[CO_2]_w$, T_a and P in the CO_2 flux across the air-water interface (left) and the ΔCO_2 (right). Air at 0.1 m s^{-1} wind and 15.8 mmol m^{-3} of CO_2 (equivalent to 370 ppm) in water at 17.38 °C, 0 ppt, 0.1 m s^{-1} current and 10 m depth. Transfer velocity (k) by double layer (DL), k_w^{wind} by McGillis (2001), α by Johnson (2010), D_w by Wilkie and Chang (1955), CD by Smith (1980) and k_a by Mackay and Yeun (1983).

OSD
9, 909–975, 2012

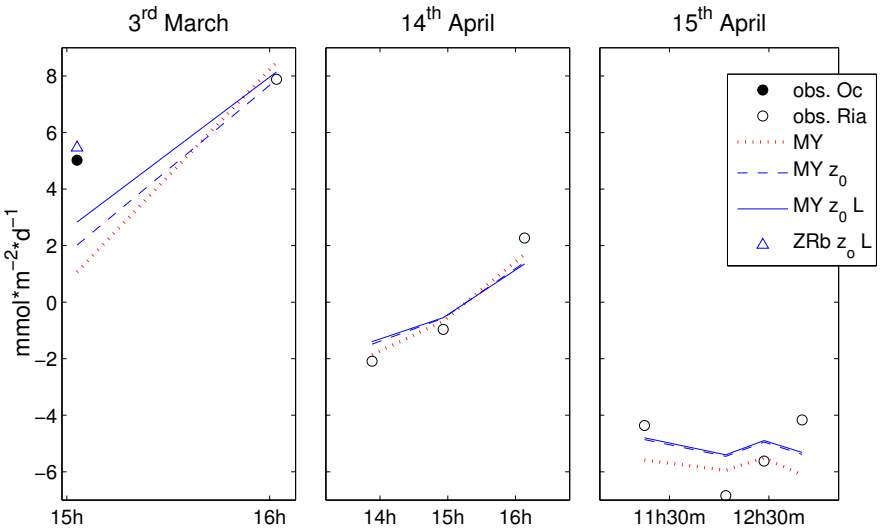

Fig. 12. CO_2 flux across the air-water interface (obs) observed (Ria) inside Ria Formosa or (Oc) in the nearby coastal ocean, and predicted by (MY) Mackay and Yeun (1983) or (ZRb) Zhao et al. (2003) with breaking wave parameter, (z_0) accounting for sea-state and (L) accounting for atmospheric stability. All: transfer velocity (k) by double layer, α by Johnson (2010), D_w by Wilkie and Chang (1955), and k_a by Mackay and Yeun (1983).

OSD
9, 909–975, 2012

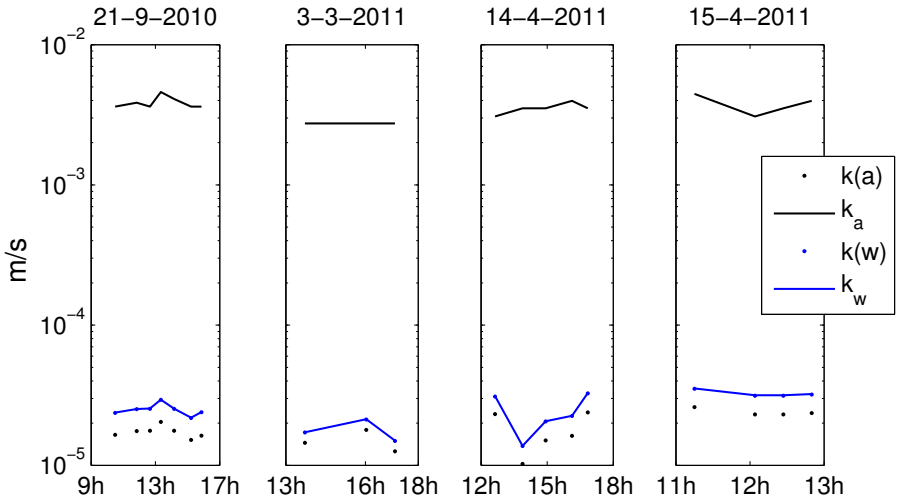

Fig. 13. Transfer velocity limiting phase. Overall transfer velocity from the air (k(a)) and from the water point of view (k(w)); air-side transfer velocity (k_a) and water-side transfer velocity (k_w).

OSD
9, 909–975, 2012

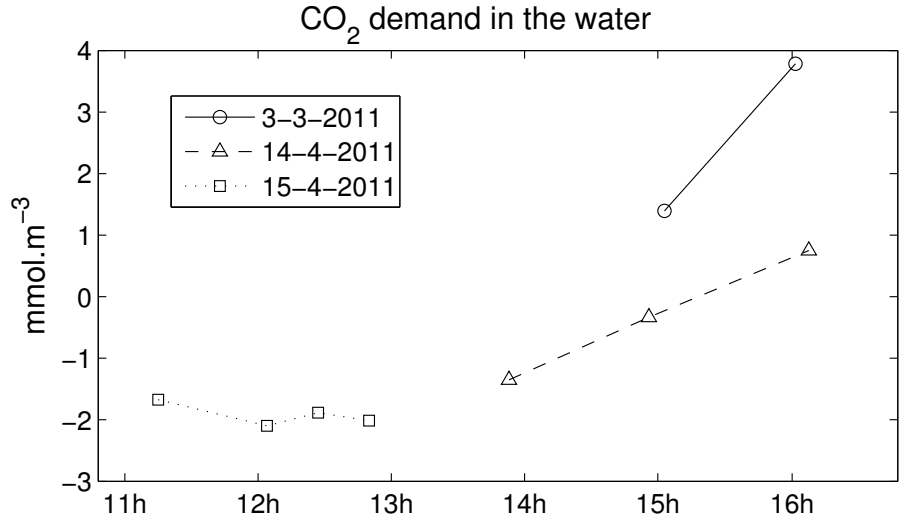

Fig. 14. ΔCO_2 for the three sampled time series.

OSD
9, 909–975, 2012

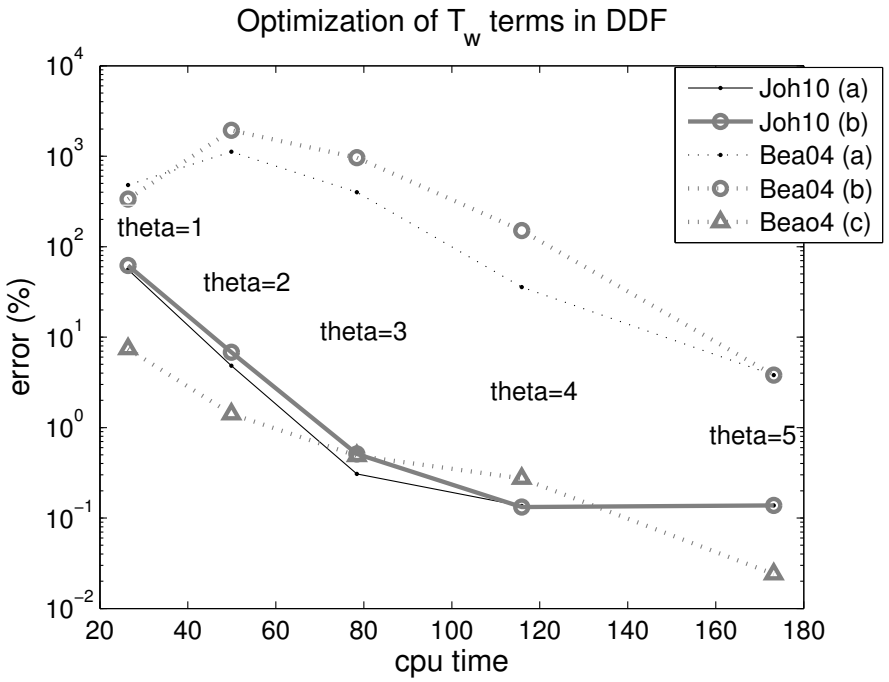

Fig. 15. Choosing n and Θ for the $T_w^\circ C$ terms in the DDF. **(a)** $n = \Theta$ and **(b)** $n = 5$. The **(a)** and **(b)** estimates with $[CO_2]$ given in ppm. **(c)** $n = \Theta$ with $[CO_2]$ given in mol m^{-3}.

OSD
9, 909–975, 2012

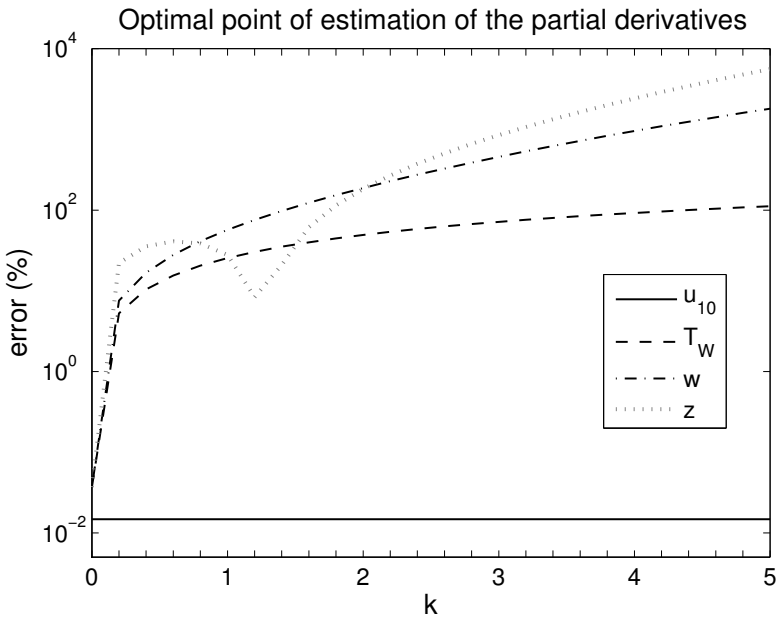

Fig. 16. Optimal k for wind speed (u_{10}), water temperature (T_w), current velocity (w) and depth (z). All $n_i = 5$ and $\Theta_i = 5$. The $\delta_4 = 2\,\mathrm{km\,h^{-1}}$ (u_{10}), $\delta_9 = 1.8\,^{\circ}\mathrm{C}$ (T_w), $\delta_{11} = 0.7488\,\mathrm{hm\,h^{-1}}$ (w) and $\delta_{12} = 1.29\,\mathrm{dam}$ (z).

OSD
9, 909–975, 2012




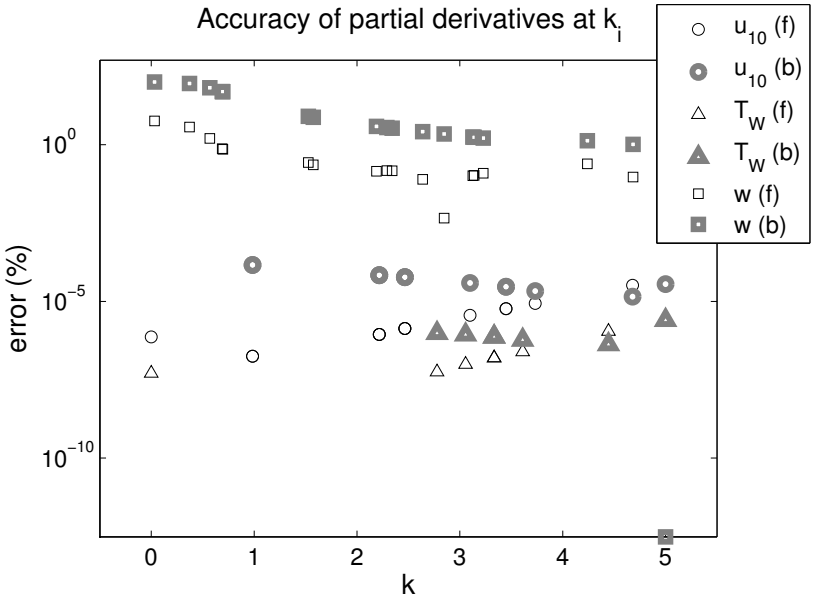

Fig. 17. Accuracy of the partial derivatives estimated at k_i located between $_{\min}x_i$ and $_{\max}x_i$. Results are shown for wind speed (u_{10}), water temperature (T_w) and current velocity (w). Derivatives estimated by (f) forward formula and (b) backward formula.

OSD
9, 909–975, 2012

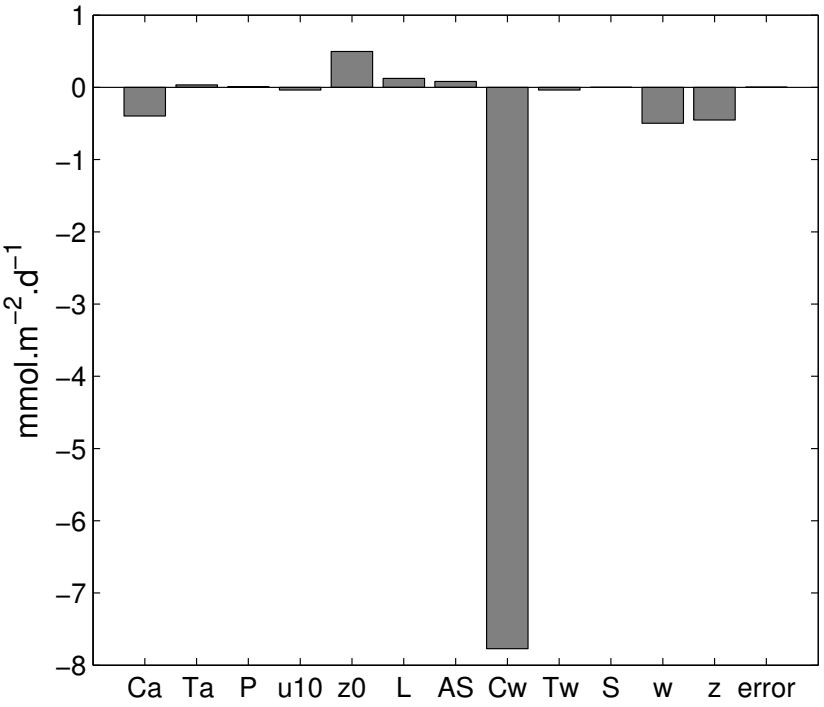

Fig. 18. Decomposition of the Difference between the CO_2 Flux in Ria Formosa at the 15 April 2011 and in the nearby coastal ocean at the 3 March 2011. Transfer velocity (k) by double layer, k_w^{wind} by Mackay and Yeun (1983), $k_w^{current}$ by O'Connor and Dobbins (1958), α by Johnson (2010), D_w by Wilkie and Chang (1955), and k_a by Mackay and Yeun (1983). Vectors n and Θ were [1 2 1 2 2 1 1 1 3 1 2 2].

OSD
9, 909–975, 2012